Research Square

Preprints are preliminary reports that have not undergone peer review.
They should not be considered conclusive, used to inform clinical practice,
or referenced by the media as validated information.

Sex-divergent microRNA–mRNA regulatory networks in the dorsolateral prefrontal cortex in major depressive disorder

Analia Bortolozzi

analia.bortolozzi@iibb.csic.es

Institute of Biomedical Research of Barcelona (IIBB), Spanish National Research Council (CSIC)
https://orcid.org/0000-0002-2069-9192

Lluis Miquel-Rio

IDIBAPS https://orcid.org/0000-0002-3547-6004

Judith Jericó-Escolar

Institute of Biomedical Research of Barcelona (IIBB), Spanish National Research Council (CSIC)

Veónica Paz

Centro de Investigación Biomédica en Red de Salud Mental (CIBERSAM), ISCIII, Madrid, Spain

Esther Ruiz-Bronchal

Institut d'Investigacions Biomèdiques de Barcelona (IIBB), Spanish National Research Council (CSIC), Barcelona, Spain

Luís F Callado

University of the Basque Country https://orcid.org/0000-0001-9941-012X

J Javier Meana

University of the Basque Country https://orcid.org/0000-0002-7913-6714

Muriel Vicent-Gil

Institut de Recerca Sant Pau (IR SANT PAU)

Maria Portella

Institut de Recerca Sant Pau (IR Sant Pau) https://orcid.org/0000-0002-2007-9516

Javier de Diego-Adeliño

Hospital de la Santa Creu i Sant Pau https://orcid.org/0000-0001-9708-2441

Gustavo Turecki

McGill University https://orcid.org/0000-0003-4075-2736

Cristina Fornaguera

Grup d'Enginyeria de Materials (Gemat), Institut Químic de Sarrià (IQS), Universitat Ramon Llull (URL).
https://orcid.org/0000-0002-7014-3213

Eduard Vieta

Universitat de Barcelona Facultat de Medicina i Ciències de la Salut https://orcid.org/0000-0002-0548-0053

Article

Keywords: Major depressive disorder, Suicide, Sex differences, MicroRNA-mRNA networks, Single-nucleus transcriptomic

Posted Date: November 2nd, 2026

DOI: https://doi.org/10.21203/rs.3.rs-11555499/v1

License: This work is licensed under a Creative Commons Attribution 4.0 International License. Read Full License

Additional Declarations: Yes there is potential Competing Interest. J.D.A. has served as consultant, advisor or CME speaker for Johnson & Johnson, Lundbeck, Pfizer, Neuraxpharm, Exeltis, Esteve and Viatris, outside the submitted work. EV has received grants and served as consultant, advisor or CME speaker for the following entities: AB-Biotics, Abbott, AbbVie, Adamed, Adium, Alcediag, Angelini, Biogen, Beckley-Psytech, Biohaven, Boehringer-Ingelheim, Bristol-Myers-Squibb, Casen-Recordati, Celon Pharma, Compass, Dainippon Sumitomo Pharma, Eli-Lilly, Engrail, Esteve, Ethypharm, Ferrer, Gedeon Richter, GH Research, Glaxo-Smith Kline, HMNC, Intra-Cellular therapies, Idorsia, Johnson & Johnson, LB pharmaceuthicals, Lundbeck, Luye Pharma, Medincell, Merck, Mitsubishi Tanabe Pharma, Newraxpharm, Newron, Novartis, Organon, Orion Corporation, Otsuka, Roche, Rovi, Sage, Sanofi-Aventis, Signant Health, Sunovion, Takeda, Teva, and Viatris, outside the submitted work. The other authors declare that they have no known competing financial interests or personal relationships that could have appeared to influence the work reported in this paper.

Sex-divergent microRNA–mRNA regulatory networks in the dorsolateral prefrontal cortex in major depressive disorder

Lluis Miquel-Rio[1], Judith Jericó-Escolar[1], Verónica Paz[1], Esther Ruiz-Bronchal[1], Luis F Callado[2], J Javier Meana[2], Muriel Vicent-Gil[3], Maria J Portella[3], Javier de Diego-Adeliño[3], Gustavo Turecki[4], Cristina Fornaguera[5], Eduard Vieta[6], and Analia Bortolozzi[1]*

[1] Institute of Biomedical Research of Barcelona (IIBB), Spanish National Research Council (CSIC), 08036 Barcelona, Spain; Translational Research Programme for Brain Disorders, Institut d'Investigacions Biomèdiques August Pi i Sunyer (IDIBAPS), Barcelona, Spain; Biomedical Research Networking Center for Mental Health (CIBERSAM), Institute of Health Carlos III (ISCIII), Madrid, Spain

[2] Department of Pharmacology, University of the Basque Country EHU, E-48940 Leioa, Bizkaia, Spain; Biobizkaia Health Research Institute, Barakaldo, Spain; Biomedical Research Networking Center for Mental Health (CIBERSAM), Institute of Health Carlos III (ISCIII), Madrid, Spain

[3] Mental Health Research Group, Institut de Recerca Sant Pau (IR Sant Pau), Barcelona, Spain; Department of Psychiatry and Legal Medicine, Universitat Autònoma de Barcelona (UAB), Spain; Department of Psychiatry, Hospital de la Santa Creu i Sant Pau (HSCSP), Barcelona, Spain; Biomedical Research Network Research Center on Mental Health (CIBERSAM), Madrid, Spain

[4] Department of Psychiatry, McGill Group for Suicide Studies, Douglas Mental Health University Institute, McGill University, Montreal, QC, Canada

[5] Grup d'Enginyeria de Materials (GEMAT), Institut Químic de Sarrià (IQS), Universitat Ramon Llull (URL), Barcelona, Spain; Institució Catalana de Recerca i Estudis Avançats (ICREA), Barcelona, Spain

[6] Bipolar and Depressive Disorders Unit, Hospital Clinic de Barcelona, Barcelona, Spain; Translational Research Programme for Brain Disorders, Institut d'Investigacions Biomèdiques August Pi I Sunyer (IDIBAPS), Barcelona, Spain; Department of Medicine, Faculty of Medicine and Health Sciences, Institute of Neurosciences (UBNeuro), University of Barcelona (UB), Barcelona, Spain; Biomedical Research Networking Center for Mental Health (CIBERSAM), Institute of Health Carlos III (ISCIII), Madrid, Spain

*Correspondence: Dra. Analia Bortolozzi, Department of Neuroscience and Experimental Therapeutics (IIBB-CSIC), Rosselló161, 08036 Barcelona, Spain, e-mail: analia.bortolozzi@iibb.csic.es

Short title: Sex-divergent miRNA-mRNA networks in depression

Keywords: Major depressive disorder; Suicide; Sex differences; MicroRNA-mRNA networks; Single-nucleus transcriptomic

Abstract

Post-mortem studies have identified transcriptomic alterations in major depressive disorder (MDD), but sex-specific post-transcriptional mechanisms remain poorly understood. Here, we profiled microRNAs and mRNAs in the dorsolateral prefrontal cortex of males and females with MDD, most of whom died by suicide, and sex-matched controls. We integrated these profiles with experimentally supported microRNA–target interactions, validated selected changes by RT-qPCR, and mapped targets using an independent single-nucleus transcriptomic dataset. Differentially expressed microRNAs were predominantly upregulated in males and downregulated in females (73% in each sex), and differentially expressed genes largely differed between sexes; most shared microRNAs and genes altered in both sexes changed in opposite directions. In males, microRNA-mRNA regulatory networks involved genes related to proteostasis and intracellular trafficking, and mapped mainly to excitatory neurons. In females, these networks involved genes related to metabolism and neuroendocrine-immune signaling, distributed across neuronal, glial, and vascular cells. These findings reveal sex-divergent post-transcriptional regulation in MDD and support sex-stratified biomarker and therapeutic research.

INTRODUCTION

Major depressive disorder (MDD) is a leading cause of disability worldwide, affecting around 280 million people and contributing to the global disease burden[1–3]. It is roughly twice as common in females as in males[3]. MDD is also a major risk factor for suicide[4]: more than 60% of individuals who attempt suicide have MDD, and people with this disorder are about 20 times more likely to die by suicide than the general population[5]. Nevertheless, most individuals with MDD do not die by suicide, and suicidal behavior differs by sex: attempts are more frequent in females, whereas deaths by suicide are more frequent in males[6–8]. Understanding the molecular mechanisms of depression and suicidal behavior in each sex is therefore a prerequisite for more precise treatments.

Converging evidence from neuroimaging and post-mortem studies implicates the dorsolateral prefrontal cortex (dlPFC) in the pathophysiology of MDD and suicide, including structural deficits and disrupted functional connectivity,[9–13] as well as widespread transcriptomic alterations[14–21]. Recent studies have begun to dissect the sex-dependent transcriptomic landscape of depression[20,22–26], but the post-transcriptional regulatory mechanisms underlying these changes, particularly those mediated by non-coding RNAs, remain poorly understood. MicroRNAs (miRNAs) are key regulators of synaptic plasticity and stress responses[27–29], and altered miRNA profiles have been described in the dlPFC of individuals with depression[30–32]. However, most of these studies did not analyze the sexes separately or integrate miRNA and mRNA data at the network level. Pooling the sexes can mask regulatory changes that differ, or even oppose each other, in males and females.

Here, we address this gap by profiling miRNA and mRNA expression in the dlPFC of 70 individuals (40 males, 30 females), comprising subjects with MDD, most of whom died by suicide, and matched controls. Differentially expressed miRNAs (DEmiRs) were predominantly upregulated in males and downregulated in females, and differentially expressed genes (DEGs) showed little overlap between sexes. Moreover, nearly all DEmiRs and most DEGs shared by both sexes changed in opposite directions. From the RT-qPCR-confirmed DEmiRs, we built miRNA–mRNA regulatory networks for each sex and validated a subset of candidate target genes. Mapping these targets onto an independent single-nucleus RNA-sequencing dataset of the human dlPFC[23] revealed distinct cellular contexts. In males, targets were related to proteostasis, intracellular trafficking, and synaptic scaffolding, and were altered mainly in superficial and deep-

layer excitatory neurons. In females, targets were related to metabolism, cytoskeletal dynamics, and neuroendocrine-immune signaling, and were distributed across neuronal, glial, and vascular cells. These findings reveal sex-divergent post-transcriptional regulation in the dlPFC in MDD and provide a basis for sex-stratified miRNA biomarker research.

RESULTS

Opposite miRNA expression changes in the dlPFC of males and females with MDD who died by suicide (MDD-S)

The main objective of this study was to determine whether miRNA-mRNA regulatory networks in the dlPFC of individuals with MDD who died by suicide (MDD-S) differ between the sexes, and to infer the cell types in which the target genes are altered (**Fig. 1**). We first performed small RNA sequencing in a discovery cohort of 34 individuals, comprising males (n=10) and females (n=7) with MDD-S and matched controls (**Tables 1, S1)**. Sequencing yielded an average of 35 million raw reads per sample, with a median Phred quality score above 30 across all bases. After deduplication based on unique molecular identifiers (UMIs), reads were mapped sequentially: they were first aligned to small RNA databases (miRBase v22.1, piRNAdb v1.7.6, tRNA v19 and snoDB v22), with mapping rates of 17.3–34.7%, and the remaining reads were then aligned to the human reference genome (GRCh38/hg38), with mapping rates of 85–90% (**Fig. S1**).

We detected 1,972 annotated miRNAs, corresponding to 73.5% of the human mature miRNAs in miRBase (v22.1). Differential expression analysis with both sexes combined identified 34 miRNAs that differed between MDD-S and controls subjects (p<0.05; 1.7% of the 1,972 detected miRNAs): 17 were upregulated and 17 downregulated. Additionally, 55 miRNAs (2.8% of the 1,972 detected miRNAs) showed marginal significances (0.05≤p<0.1) (**Fig. S2, Table S2, Supplementary Data 1**).

Sex-stratified analysis showed markedly different miRNA changes in males and females with MDD-S relative to sex-matched controls (**Figs. 2a-f, Tables S3, S4**). In males, we identified 129 differentially expressed miRNAs (DEmiRs; 6.5% of total detected, p<0.05), of which 94 (73%) were upregulated and 35 (27%) downregulated (**Figs. 2a-c**). Females showed the opposite pattern: of 92 DEmiRs (4.7% of total sequenced, p<0.05), 67 miRNAs (73%) were downregulated and 25 (27%) upregulated

(**Figs. 2d–f**). Furthermore, 97 miRNAs in male and 71 in females showed marginal differences ($0.05 \leq p < 0.1$). Forty DEmiRs were shared between the sexes, and 38 of these (95%) changed in opposite directions: 35 were upregulated in males and downregulated in females, and 3 were downregulated in males and upregulated in females. The remaining two changed in the same direction in both sexes (**Fig. 2g, Tables S3, S4**). Rank-rank hypergeometric overlap (RRHO2) analysis and Spearman's correlation[33] showed that this inverse relationship extended across the miRNome, with MDD-S associated miRNA effect sizes negatively correlated between males and females (ρ=-0.3859; $p=1.5\times10^{-61}$, **Fig. 2h**).

Next, we prioritized 37 miRNAs (**Figs. S3, S4**) based on read abundance, fold-change (>20%), documented expression in the brain, and reported disease associations (HMDD v4.0)[34]. All of them had also been detected in plasma samples from MDD patients enrolled in a cognitive remediation trial (NCT07014683)[35]. RT-qPCR measurements correlated with miRNA-seq expression for 31 of the 37 miRNAs (23 significant, $p<0.05$, and 8 marginal, $0.05 \leq p < 0.10$), whereas no correlation was found for miR-126-5p, miR-199a-5p, miR-33a-3p, miR-574-5p, miR-5584-5p, and miR-6734-5p (**Fig. S5**). We next assessed whether miRNA expression was associated with potential biological and technical confounders. Most miRNAs showed no association with age, post-mortem interval (PMI) or RNA integrity number (RIN). Nominal associations ($p<0.10$) were observed for 4 miRNAs with age (2 with $p<0.05$), 7 with PMI (4 with $p<0.05$) and 6 with RIN (3 with $p<0.05$) (**Figs. S6–S8**). Thus, the observed differences are unlikely to be driven by these variables.

RT-qPCR in an extended cohort confirms opposite miRNA changes in males and females

To confirm these sex differences, the miRNAs selected from the technical validation in each sex (15 miRNAs in males and 13 in females) were measured by *de novo* RT-qPCR in that sex in an extended cohort. This cohort added dlPFC samples from 10 males and 8 females with MDD, together with matched controls, to the discovery samples (**Table S1**). All males with MDD had died by suicide (MDD-S; n=20), whereas the females with MDD (n=15) included individuals who died by suicide (MDD-S; n=9) or from natural causes (MDD-N; n=6), hereafter MDD-S/N. In males, all 15 miRNAs were confirmed as DEmiRs, most of which were upregulated (let-7b-3p, let-7b-5p, miR-100-5p, miR-151a-5p, miR-151b, miR-181a-3p, miR-21-5p, miR-27b-3p, miR-320c, miR-499a-5p, miR-

625-5p, and miR-642a-5p); only three (miR-195-5p, miR-199a-5p, and miR-4516) were downregulated (**Fig. 3a**). In females, all 13 miRNAs were confirmed as DEmiRs, most of which were downregulated (miR-151a-5p, miR-151b, miR-219a-2-3p, miR-23b-3p, miR-27b-5p, miR-423-5p, miR-4516, miR-483-5p, miR-625-5p, and miR-642a-5p); only three (miR-126-5p, miR-187-3p, and miR-378a-3p) were upregulated (**Fig. 4a**). We then asked whether miRNA expression in females differed according to cause of death. Bayesian equivalence test provided moderate evidence that MDD-S and MDD-N females did not differ in any of the 13 DEmiRs (BF_{01}=3.4-5.6; robust across prior widths; **Fig. S9**), indicating that, in females, these changes are associated with MDD irrespective of suicide. Five DEmiRs were confirmed in both sexes (miR-151a-5p, miR-151b, miR-4516, miR-625-5p, and miR-642a-5p). Four of them changed in opposite directions, being upregulated in males and downregulated in females, whereas miR-4516 was downregulated in both.

To explore the biological functions associated with these miRNAs, we performed KEGG and Gene Ontology (GO) enrichment analyses of the experimentally supported targets of the DEmiRs confirmed in each sex, covering biological processes (GO_BP) and molecular functions (GO_MF). In both sexes, targets were enriched in cellular senescence (*p.adj*=6.36×10^{-17} in males and 1.32×10^{-12} in females), FoxO signaling (*p.adj*=6.14×10^{-16} and 1.0×10^{-7}), MAPK signaling (*p.adj*=3.78×10^{-11} and 5.89×10^{-8}), and neurotrophin signaling (*p.adj*=1.01×10^{-11} and 1.0×10^{-7}) pathways (**Figs. 3b,c, 4b,c, Supplementary Data 2**). The enriched GO_BP terms, however, differed between sexes. In males, enriched terms included protein localization to the nucleus (*p.adj*=7.88×10^{-13}), nuclear transport (*p.adj*=4.82×10^{-12}), response to endoplasmic reticulum (ER) stress (*p.adj*=2.52×10^{-6}), and autophagy regulation (*p.adj*=9.87×10^{-9}) (**Fig. 3d)**. In females, enriched terms included endocrine system development (*p.adj*=8.76×10^{-5}), response to peptide hormone (*p.adj*=8.95×10^{-4}), immune system development (*p.adj*=1.15×10^{-3}), NF-κB-driven immune mobilization (*p.adj*=1.49×10^{-4}), and neuron differentiation (*p.adj*=2.53×10^{-4}) (**Fig. 4d)**. GO_MF terms showed a similar pattern. Terms as ubiquitin-like protein ligase, SMAD, and β-catenin binding were enriched in both sexes. Male-only enriched terms included binding to signaling and scaffolding proteins (e.g., tau, p53, and 14-3-3 binding) and kinase activity, whereas female-specific terms were related to transcription and translation (e.g., DNA-binding transcription factor binding, diverse RNA binding, and translation regulator activity) (**Figs. 3e, 4e**). Thus, although the targets of male and female DEmiRs converged on shared signaling pathways, they were

associated with different biological processes: proteostasis, stress responses and protein scaffolding in males, and neuroendocrine-immune signaling and gene expression regulation in females.

Gene expression changes in the dlPFC are largely sex-divergent and partially inverse in MDD-S

We next examined mRNA expression in the discovery cohort. Reads not assigned to small RNA databases (65.3-82.7% reads per sample) were quantified with featureCounts (v2.0.1)[36], yielding 12,173 detected genes, with comparable transcriptome coverage in both sexes (~63.9% of annotated brain protein-coding genes). Using a nominal threshold (p<0.05), MDD-S males showed 1,057 DEGs (8.7% of detected genes), of which 59% were upregulated and 41% downregulated. MDD-S females showed 1,143 DEGs (9.4%), of which 86% were downregulated and 14% upregulated (**Figs. 5a–f, Supplementary Data 3**). Most DEGs were altered in only one sex (956 of 1,057 in males and 1,042 of 1,143 in females). The 101 DEGs shared by both sexes did not exceed the overlap expected by chance (~105; hypergeometric test, p=0.94). However, 77 of them (76%) changed in opposite directions, more than expected from the proportions of up- and downregulated DEGs in each sex (~57; two-sided exact binomial test, $p=4.8\times10^{-5}$). Only 24 DEGs changed in the same direction, 1 upregulated and 23 downregulated (**Fig. 5g, Table S5**). Most shared DEGs were autosomal; three were X-linked (*CSTF2, LAMP2, SRPX2*), and none were Y-linked. RRHO2 analysis and Spearman's correlation[33] showed that this inverse relationship extended across the transcriptome: differential expression statistics negatively correlated between males and females (ρ=-0.21; $p=9.24\times10^{-102}$; **Fig. 5h**). A similar pattern was observed in an independent bulk RNA-seq dataset of the dlPFC[22], in which MDD-associated changes were also predominantly discordant between sexes (ρ=-0.10; $p=1.77\times10^{-37}$; **Fig. S10**).

Functional enrichment analysis of the 101 shared DEGs was exploratory, as no term reached FDR<0.05 (**Table S6, Supplementary Data 4**). The top-ranked terms included protein folding (p=0.008; e.g., *FKBP11, HSPA9, PPIF, CALR, PDIA4*), protein processing in the ER (p=0.016; e.g., *CALR, RRBP1, SSR1, PDIA4*), hormone-mediated signaling (p=0.005; e.g., *KDM1A, NR2C1, CALR, LANCL2, PRMT2*), intracellular receptor signaling (p=0.019; e.g., *NR2C1, NR2C2, STAT3, KDM1A, CALR, PRMT2)*, and neurodevelopment (e.g., neural tube development; p=0.013; *MARCKS, ITPK1, SSBP3,*

VANGL2). Because most shared DEGs changed in opposite directions, these terms indicate processes affected in both sexes rather than changes common to both.

DEGs found only in males (n=956) were enriched in pathways associated to intracellular transport and synaptic organization. Enrichment terms included Golgi vesicle transporter ($p_{.adj}$<0.003), vacuolar transport (p=6.42×10^{-4}), synapse organization ($p_{.adj}$<0.01), glutamate receptor signaling ($p_{.adj}$<0.035) and glutamatergic synapse (p<0.01), the latter including genes encoding postsynaptic density and scaffolding proteins. Protein processing in the ER was also represented with 24 male-only DEGs in this pathway compared to 4 shared DEGs. Further, enriched terms included RNA splicing ($p_{.adj}$< 0.01) and RNA localization (p= 4.6×10^{-4}). Among molecular functions, male-only DEGs were enriched in ribonucleoprotein complex binding (p=6.21×10^{-4}), ubiquitin-like protein ligase binding (p<0.003) and GTPase activity (p=0.0045) (**Figs. 6a-6c)**.

DEGs found only in females (n=1,042) were enriched in lipid metabolism, nuclear transport, and signaling pathways related to inflammation. Enriched pathways included fatty acid metabolism ($p_{.adj}$<0.0011), biosynthesis of unsaturated fatty acids (p=0.0038), and nucleocytoplasmic transport (p=0.0014). Female-only DEGs were also enriched in GABAergic synapse (p=0.0051) and GABA receptor activity (p=0.038), as well as MAPK (p=0.0026), TGF-β (p=0.0095), and NFκB (p=0.0029) signaling pathways. Among molecular functions, they were enriched in ubiquitin-like protein ligase binding ($p_{.adj}$<0.015) and protein–macromolecule adaptor activity ($p_{.adj}$< 0.016) (**Figs. 6d-6f**).

Thus, several biological processes were affected in both sexes, but through largely different genes: in 35 GO biological processes enriched in both male-only and female-only DEGs, the annotated genes were predominantly upregulated in males (31 of 35 terms) and downregulated in females (all 35 terms) **(Fig. 6g, Table S7**).

Sex-divergent miRNA-mRNA regulatory networks in the dlPFC

To identify sex-specific post-transcriptional regulation in MDD-S, we combined the DEmiRs confirmed by RT-qPCR and the DEGs from each sex with experimentally supported miRNA-target interactions from miRTarBase[37]. Because miRNAs typically repress their gene targets[38], we retained miRNA–mRNA pairs in which the miRNA and its target changed in opposite directions. The male network comprised 15 DEmiRs and 147 validated target DEGs: 12 upregulated DEmiRs targeting 103 downregulated DEGs, and 3 downregulated DEmiRs targeting 44 upregulated DEGs (**Figs. 7a,b)**. Of the 13 female DEmiRs, 12 had validated targets among the female DEGs, yielding a network of

49 target DEGs: 3 upregulated DEmiRs targeting 33 downregulated DEGs, and 9 downregulated DEmiRs targeting 16 upregulated DEGs. The remaining DEmiR, miR-151b, had no target among the female DEGs (**Figs. 8a,b)**.

The male and female networks differed in structure. In the male up-miRNA/down-mRNA network, let-7b-5p, miR-21-5p, and miR-320c were the most connected miRNAs (**Fig. 7a**), whereas the corresponding female-associated up-miRNA/down-mRNA network was small and centered on miR-378a-3p and miR-126-5p (**Fig. 8a**). *NR2C2* was downregulated in both sexes, but was linked to different miRNAs: miR-21-5p in males and miR-126-5p in females (**Figs. 7c, 8c**). In males, 27 target mRNAs were linked to two or more DEmiRs (e.g., *CBX6* to miR-151b, miR-151a-5p, and miR-642a-5p; **Fig. 7c**). In females, most targets were linked to a single DEmiR, the exceptions being *WNK1* (miR-378a-3p and miR-126-5p) and *MNT* (miR-378a-3p and miR-187-3p) (**Fig. 8c**).

The down-miRNA/up-mRNA regulatory networks showed a similar contrast (**Figs. 7b, 8b)**. In males, miR-195-5p was the main hub and shared targets with miR-4516 and miR-199a-5p. The male network targets included genes involved in cell cycle regulation and signaling (e.g., *ERBB2*, *HIF1A*, *INSR*, and *STAT3*), and some were linked to two DEmiRs (e.g., *CANX*, *DDX3X*, and *ARHGAP12*) (**Figs. 7b,c**). In females, the down-miRNA/up-mRNA network had no dominant hub and consisted of small, separate modules such as miR-625-5p with its targets *COL1A2* and *SMC1A.* A few candidate targets were linked to two DEmiRs (e.g., *SMYD2* to miR-4516 and miR-27b-5p*;* and *RGS5* to miR-23b-3p and miR-642a-5p), but most interactions involved a single miRNA-target pair (e.g., miR-483-5p and *MLXIP*) (**Figs. 8b,c**).

We next mapped the target genes onto physical protein-protein interaction (PPI) networks and identified the most densely connected clusters[39,40]. In males, the main clusters were related to stress-proteotoxicity and G-protein coupled receptor (GPCR) signaling modules (**Fig. 7d**). The most connected node, HSPA5 (BiP; degree k=11), formed a cluster with chaperones and cell-cycle regulators (CDKN1A, MAPK14, EEF1A1), and a second cluster includes the G-protein signaling components GNB1, GNAQ, and ADCY1. In females, the PPI network was less interconnected, and its main cluster was centered on NR2C2, which connected metabolic regulators (NCOA3 and ACACA) with structural and transport proteins (SMC1A and KIF1B) (**Fig. 8d**). NR2C2 was present in the PPI networks of both sexes, but linked to different partners: stress-related proteins in males (k=9) and metabolic and cytoskeletal proteins in females (k=6).

Based on these networks and on miRNA binding sites in the target transcripts (**Fig. S11**), we selected candidate target genes and quantified their expression by RT-qPCR in the extended cohort (**Figs. 7e, 8e, S12, S13**). *NR2C2* mRNA was downregulated in both sexes, and its levels correlated inversely with miR-21-5p in males and with miR-126-5p in females (**Figs. 7e,f, 8e,f**). In MDD-S males, *EEF1A1, SATB1,* and *CELF2* were downregulated, and *CANX* was upregulated (**Fig. 7e**). Their expression correlated inversely, either significantly or marginally, with: let-7b-5p/miR-100-5p, miR-100-5p/miR-21-5p, miR-27b-3p/miR-642a-5p, and miR-195-5p/miR-4516, respectively (**Fig. 7f**). In females with MDD-S/N, *SMYD2* and *MCTP1* were upregulated, *RGS5* showed a marginal increase, and *ID2* was downregulated (**Fig. 8e**). Their mRNA levels correlated inversely (significantly or marginally) with miR-27b-5p/miR-4516, miR-642a-5p, miR-23b-3p/miR-642a-5p, and miR-378a-3p, respectively (**Fig. 8f**). In females, Bayesian equivalence tests provided moderate evidence that MDD-S and MDD-N subjects did not differ for any of the five genes (BF_{01}=3.3–5.5 with the reference prior; 2.7–11.7 across prior widths; **Fig. S14**). Thus, these changes appear to be associated with MDD irrespective of suicide. None of the four genes altered in males differed significantly in females, and *viceversa* (**Fig. S15**). To test formally whether MDD-associated changes differed between the sexes, we performed a sex-by-diagnosis interaction analysis for all protein-coding genes detected in both sexes **(Table S8, Supplementary Data 5**). Among the RT-qPCR-validated genes, the interaction was significant for *CANX*, which was changed in males, and for *SMYD2, MCTP1, RGS5*, and *ID2*, which were altered in females. It was marginal for *SATB1* (p=0.057) and not significant for *EEF1A1* or *CELF2*. Sex specificity was therefore statistically supported for five of the eight genes altered in only one sex.

Candidate target genes map to different dlPFC cell populations in males and females

To infer the cell types in which candidate target genes are changed, we projected the candidate targets of DEmiRs in a large-scale human dlPFC snRNA-seq dataset (GEO: GSE213982; n=160,711 nuclei, 51% from female)[23]. Using the cell-type annotations and differential expression procedures of the original study[23], we identified, separately for each sex, the clusters in which candidate genes were differentially expressed (Bonferroni-adjusted<0.05; **Figs. 9a,b, Supplementary Data 6**). Of the 147 male and 49 female network targets, 41 and 26, respectively, were differentially projected in at least one cluster. In males, these candidate genes were found mainly in excitatory neurons of the

upper and deep cortical layers (ExN1_L24, ExN10_L46, ExN2_L23), where most were downregulated. In females, they were distributed more evenly across excitatory clusters, with ExN2_L23 contained the largest number and similar proportions of up- and downregulated genes. In both sexes, candidate genes were also differentially projected in parvalbumin interneurons (InN1_PV), astrocytes (Ast), and oligodendrocytes (Oli), whereas changes in endothelial cells and mixed-lineage clusters were detected only in females (**Figs. 9a,b**). Overall, 61.0% of the male candidate genes (25/41) were downregulated, and 58.5% (24/41) were differentially expressed in a single cell type. Among female candidate genes, 46.2% (12/26) were downregulated and 53.8% (14/26) upregulated, and 61.5% (16/26) were differentially expressed in more than one cluster (**Fig. 9c**).

We then examined the distribution of RT-qPCR-tested candidates across the 41 reference clusters[23] (**Figs. 9d,e**). In males, these included regulators of protein homeostasis and chromatin structure. *EEF1A1* was downregulated in three excitatory clusters (ExN10_L46, ExN2_L23, and ExN3_L46) and one inhibitory (InN4_VIP), but upregulated in ExN1_L24. *CANX* was downregulated in ExN10_L46, ExN2_L23, and InN1_PV, and the chromatin organizer *SATB1* was downregulated in five neuronal clusters (ExN10_L46, ExN2_L23, ExN3_L46, InN1_PV, and InN5_SST). Whereas these target genes were altered mainly in neurons, particularly excitatory neurons of layers 2-6, *CELF2* was upregulated in both neuronal (ExN10_L46, ExN2_L23, and ExN3_L46) and glial clusters (Ast1 and Oli1) (**Fig. 9d)**.

In females, *MCTP1* was altered, mainly upregulated, in eight clusters, including excitatory neurons (ExN10_L46, ExN17, ExN3_L46, and ExN7), astrocytes (Ast1), and oligodendrocytes (Oli1-3). *SMYD2* was upregulated in ExN2_L23; *ID2* was downregulated in five excitatory clusters (ExN1_L24, ExN17, ExN2_L23, ExN3_L46, and ExN6), but upregulated in astrocytes (Ast1 and Ast2); and *RGS5* was downregulated in an endothelial cluster (End1) (**Fig. 9e).** By contrast, *NR2C2*, which was downregulated in both sexes in bulk tissue, did not reach significance in any cluster in either sex**.** Thus, in this independent dataset, male candidate genes were altered mainly in excitatory neurons, recurrently the same excitatory cluster, whereas female candidate genes were altered across neuronal, glial and vascular cells.

DISCUSSION

Here, we show that MDD is associated with largely distinct and often opposite post-transcriptional changes in the dlPFC of males and females. These findings extend previous evidence of sex differences in the transcriptional architecture of MDD[20,22–24,26] to the post-transcriptional level. Co-expression approaches such as WGCNA have linked sex-specific transcriptional modules to clinical phenotypes[24], but because these modules are built from undirected correlations, such approaches cannot by themselves identify the upstream regulators that may drive them. Directed miRNA–target networks, an approach well established in oncology and neurodegeneration research[41–45], help address this limitation. Our networks identified candidate regulators that implicate distinct biological processes in each sex. Moreover, in an independent snRNA-seq dataset, candidate target genes identified in males were altered mainly in excitatory neurons, whereas those identified in females were altered across neuronal, glial and vascular cell types.

Previous studies have documented alterations of the dlPFC miRNome in depression[29,32], but most did not consider sex as a biological variable. Our data suggest that this omission matters. Nearly all miRNAs altered in both sexes changed in opposite directions, and effect sizes were negatively correlated between males and females across the miRNome, indicating that the pattern is not restricted to transcripts that passed our significance threshold. Opposing effects can therefore cancel out when the sexes are analyzed together. This is consistent with the smaller number of DEmiRs detected in our sex-pooled comparison and may contribute to the heterogeneity of miRNA signatures reported in mixed-sex cohorts[30,46]. The mRNA data showed the same pattern, with few genes altered concordantly in both sexes. The consistency of this directional pattern across miRNAs and mRNAs suggests that largely distinct molecular pathways are engaged in the male and female dlPFC in MDD.

In males with MDD-S, the predominantly upregulated DEmiRs were associated with downregulated gene networks related to proteostasis, intracellular trafficking and synaptic scaffolding. Enrichment and PPI analyses converged on the ER stress response, with the chaperone HSPA5 (BiP), a central regulator of the unfolded protein response, as the main network hub. The most highly connected miRNAs in the male network (upregulated let-7b-5p, miR-21-5p and miR-320c; downregulated miR-195-5p) targeted molecular chaperones and translation elongation factors. Besides *NR2C2,* three RT-qPCR-validated genes were experimentally supported targets of two upregulated DEmiRs

each: *EEF1A1*, an elongation factor involved in local synaptic protein synthesis and dendritic spine remodeling[47] (let-7b-5p/miR-100-5p); *SATB1,* a chromatin organizer[48] (miR-100-5p/miR-21-5p); and *CELF2*, an RNA-binding protein that regulates the alternative splicing and stability of synaptic mRNAs[49] (miR-27b-3p/miR-642a-5p). These changes are consistent with impaired synaptic protein synthesis and chromatin regulation, although the sex-by-diagnosis interaction was only marginal for *SATB1* and not significant for *EEF1A1* or *CELF2,* so these changes may not be strictly male-specific. By contrast, *CANX* (calnexin), a target of the downregulated miR-195-5p and miR-4516, was upregulated, with a significant sex-by-diagnosis interaction. Because calnexin is an ER chaperone involved in glycoprotein folding and calcium homeostasis[50], this increase may reflect a response to ER stress rather than a loss of folding capacity. The sequencing data also pointed to reduced expression of the vesicular trafficking genes *RAB11FIP4*, a Rab11 effector in endosome recycling[51], and *ITSN2*, a scaffolding protein for clathrin-mediated endocytosis[52], and to changes in regulators of synaptic structure, including upregulation of *ARHGAP12*, required for dendritic spine morphogenesis[53], and downregulation of *ADGRL1*, a presynaptic adhesion receptor involved in excitatory synapse formation[54,55]. Cell-type mapping[23] indicated that male candidate genes are altered predominantly in superficial- and deep-layer excitatory neurons. Because these neurons are essential for cortical connectivity, ER stress and altered synaptic scaffolding in these populations could contribute to the cognitive inflexibility and impulsivity that have been associated with suicidal behavior in males[23,25,56,57].

In females, by contrast, DEmiRs were predominantly downregulated, and the associated networks converged on bioenergetics, cytoskeletal dynamics and neuroendocrine-immune signaling rather than on proteostasis. The RT-qPCR-confirmed miRNA changes did not differ between females who died by suicide and those who died from natural causes, and the same was true for the validated target genes, suggesting that the female signature is associated with MDD rather than with suicide itself. Despite the overall downward shift, the larger of the two female networks was organized around two upregulated miRNAs, miR-378a-3p and miR-126-5p, whose targets included the downregulated transcriptional regulators *ID2* (miR-378a-3p) and *NR2C2* (miR-126-5p). In parallel, downregulated miRNAs were linked to increased expression of three genes: *SMYD2*, a lysine methyl-transferase implicated in epigenetic stress responses[58,59] (miR-27b-5p/ miR-4516); *RGS5*, a regulator of G-protein signaling at vascular–immune interfaces[60,61] (miR-23b-3p and miR-642a-5p), although its increase was marginal; and

MCTP1, a calcium-binding protein involved in presynaptic vesicle trafficking[62] (miR-642a-5p). The sequencing data also pointed to altered expression of genes involved in mitochondrial and lipid metabolism (e.g., *COX6A1, ECH1,* and *ACACA*). Together, these changes are consistent with disturbed metabolic homeostasis, presynaptic function, and vascular–immune signaling. Cell-type mapping indicated a broad distribution of female candidate genes, most of which were altered in more than one cluster across neurons, astrocytes and oligodendrocytes, with endothelial changes detected only in females. This pattern is compatible with models proposing that inflammatory responses and hormone-dependent glial dysfunction contribute to depression in females[63–65].

Directed regulatory networks can also reveal how a change shared by both sexes may arise through different regulatory routes. *NR2C2* (TR4), an orphan nuclear receptor involved in protection against oxidative stress and in energy metabolism[66,67], was the only validated target downregulated in both sexes. Its levels correlated inversely with miR-21-5p in males and with miR-126-5p in females, suggesting that the same change may be linked to different miRNAs in each sex. In the PPI networks, NR2C2 was connected to stress-related proteins in males and to metabolic and cytoskeletal proteins in females, although these differences partly reflect the different gene sets from which each network was built. Functional studies will be needed to determine whether reduced *NR2C2* expression contributes to MDD and whether it could be a therapeutic target in both sexes.

Because miRNAs are relatively resistant to RNase degradation and stable in peripheral biofluids, they are attractive candidates for blood-based biomarkers[68,69]. All RT-qPCR-confirmed DEmiRs had previously been detected in plasma from individuals with MDD[35], but our data indicate that sex should be taken into account when evaluating them. Four miRNAs altered in both sexes (miR-151a-5p, miR-151b, miR-625-5p, and miR-642a-5p) changed in opposite directions in males and females; therefore, biomarker or therapeutic strategies based on them would need to be sex-specific. By contrast, miR-4516 was downregulated in both sexes. Reduced miR-4516 levels have been reported in cerebrospinal fluid extracellular vesicles from individuals with MDD who died by suicide[70], and its plasma levels increased after cognitive remediation in patients with MDD[35]. Both findings are consistent with the reduction we observed in the dlPFC and make miR-4516 a candidate peripheral marker for both sexes. However, mirroring the case of *NR2C2*, the same miRNA change was linked to different targets in each sex: together with miR-195-5p, miR-4516 targeted *CANX* in males, whereas together with miR-27b-5p it targeted *SMYD2* in females. Its downstream effects in the dlPFC may

therefore differ between the sexes. Whether brain and peripheral miR-4516 levels are correlated remains to be determined.

For some candidate genes, the direction of change differed between our bulk data and the snRNA-seq reference dataset[23]. In males, *CANX* was upregulated in bulk tissue (RNA-seq and RT-qPCR) but downregulated in two excitatory clusters and in PV interneurons in the reference data, whereas *CELF2* was downregulated in male bulk tissue but upregulated in neuronal and glial clusters. In females, *RGS5* was marginally upregulated in bulk tissue but downregulated in the End1 cluster and *ID2*, which was downregulated in bulk tissue, changed in opposite directions across cell-types (downregulated in excitatory neurons and upregulated in astrocytes). Several factors may explain these discrepancies. First, the two datasets come from independent cohorts that differ in clinical composition, tissue handling and sequencing approach. Second, snRNA-seq measures nuclear transcripts, whereas bulk tissue also captures cytoplasmic mRNAs, including those in neurites and synapses. Because miRNAs act mainly on cytoplasmic mRNAs, changes in miRNA-mediated repression can alter total transcript levels without corresponding changes in nuclear RNA. Thus, an increase in total *CANX* mRNA is compatible with reduced nuclear *CANX* transcripts in some neuronal populations if its repression by the downregulated miR-195-5p and miR-4516 is relieved. Conversely, enhanced repression of *CELF2* by the upregulated miR-27b-3p and miR-642a-5p could lower total *CELF2* mRNA despite increased nuclear levels. Third, bulk changes integrate signals from all cell types and can reflect shifts in cellular composition or opposite changes in different cell types, as observed for *ID2*. This is particularly relevant for *RGS5*, which is expressed predominantly in pericytes and other vascular cells[71] that are underrepresented in single-nucleus datasets[23,72]. Finally, cluster-level differential expression has limited statistical power for small cell populations, and the *RGS5* change in our cohort was marginal. Cell-type assignments of individual genes should therefore be regarded as provisional until confirmed by *in situ* hybridization, spatial transcriptomics or single-nucleus profiling of the same samples.

This study has several limitations. First, the discovery cohort was modest, and differential expression was defined at nominal significance thresholds. The exact numbers and proportions of DEmiRs and DEGs should therefore be interpreted with caution, although the directional patterns were supported by transcriptome-wide effect-size correlations and by RT-qPCR in an extended cohort. Because the extended cohort included the discovery samples, this validation is not fully independent. Second, all males

with MDD died by suicide, whereas the extended female cohort included both suicide and natural deaths. In females, DEmiR expression, and that of most validated target genes, did not differ between these subgroups, but we could not test whether the same holds in males, and the respective contributions of depression and suicide to the male signature remain to be determined. Third, mRNA levels were quantified from small RNA libraries, using reads that did not map to small RNA databases. This approach provides lower coverage than conventional RNA-seq, and the mRNA results, and the networks built on them, should be confirmed with dedicated RNA-seq. Fourth, although the sex-by-diagnosis interaction was tested for all protein-coding genes, it was significant for only a subset of them, including five of the eight validated genes with sex-specific changes. For the remaining genes, a significant change in one sex but not the other does not by itself establish sex specificity. Fifth, our networks rely on experimentally supported interactions from miRTarBase, which are biased toward well-studied miRNAs and genes and were largely obtained in non-neural systems. The proposed miRNA–target interactions, and the network topologies derived from them, therefore require experimental confirmation in human neural cells. Sixth, cell-type mapping relied on an independent snRNA-seq dataset and is correlative. Finally, post-mortem studies provide a cross-sectional view[73], and detailed antemortem clinical information, including treatment history, symptom severity and comorbidities, was not available. We therefore cannot distinguish primary changes from secondary consequences of chronic illness or medication.

In conclusion, integrated miRNA–mRNA profiling of the dlPFC indicates that MDD is associated with largely distinct, and often opposite, post-transcriptional changes in males and females. In males, candidate target genes were involved in proteostasis and synaptic scaffolding and mapped mainly in excitatory neurons. In females, they were involved in neuroendocrine-immune signaling and metabolic processes, and were altered across neuronal, glial and vascular cells. These findings support analyzing the sexes separately in molecular studies of depression and identify candidate miRNAs and target genes for the future development of sex-informed biomarkers and therapeutic strategies.

METHODS

Postmortem human brain samples and cohort characterization

Postmortem samples from the dorsolateral prefrontal cortex (dlPFC; Brodmann area 9) were obtained from the Basque Institute of Legal Medicine (Bilbao, Spain). Sample collection and processing complied with Spanish Biomedical Research Legislation (Law 14/2007 and RD 1716/2011) and with the Declaration of Helsinki. The study was approved by the Ethics Committee of the Spanish National Research Council (CSIC; approval no. 118/2021 Ref. PID2019-105136RB-I00). The cohort comprised 70 subjects of European descent, with 35 subjects with major depressive disorder (MDD) and 35 control subjects (20 males and 15 females per diagnostic group). Each MDD subject was matched to a control subjected of the same sex and for age at death, post-mortem interval (PMI), and RNA integrity number (RIN). A two-stage design was used. RNA sequencing was performed in a discovery cohort of 34 subjects: 17 MDD subjects who died by suicide (MDD-S) and 17 matched controls, forming 10 male and 7 female case-control pairs. Selected findings were then validated by RT-qPCR in an extended cohort of 70 subjects (35 pairs), which included the 34 discovery samples and 36 additional samples. MDD was diagnosed according to DSM-IV or DSM-IV-TR criteria after review of antemortem medical and psychiatric records. All males with MDD died by suicide (MDD-S, n = 20). The female MDD group included subjects who died by suicide (MDD-S, n = 9) and subjects who died from natural causes (MDD-N, n = 6). Control subjects had no history of neuropsychiatric disorders and died from accidental or natural causes. Toxicological screening was performed on postmortem blood samples from all subjects. Control subjects with evidence of psychotropic medications or illicit drugs were excluded, and the presence of antidepressants was recorded in MDD subjects. Neuropathological examination excluded neurodegenerative disease, head injury, and major structural brain abnormalities in all subjects. dlPFC samples (500-700 mg) were dissected by pathologists, snap-frozen, and stored at -80 °C. To ensure sample homogeneity, tissue was pulverized on dry ice without thawing and divided into aliquots of ~50 mg for RNA isolation. Demographic and clinical characteristics are summarized in **Table 1 and S1**.

RNA isolation

Total RNA, including the small RNA fraction, was isolated from dlPFC tissue aliquots using the miRNeasy Mini Kit (QIAGEN, Hilden, Germany) according to the

manufacturer's instructions. This protocol recovers both long (>200 nt) and small (<200 nt) RNAs from the same sample. RNA concentration and purity were assessed by spectrophotometry (NanoDrop; Thermo Fisher Scientific, Waltham, MA, USA), and only samples with A260/280 ≥ 1.8 and A260/230 ratios ≥ 2.0 were used. RNA integrity was assessed with Agilent TapeStation (Agilent Technologies).

Small RNA library construction and sequencing

Small RNA sequencing of the discovery cohort samples (all with RIN > 5.0) was performed by QIAGEN Genomic Services (Hilden, Germany). Libraries were prepared from 100 ng of total RNA using the QIAseq miRNA Library Kit (QIAGEN). After 3′ and 5′ adapter ligation, RNA was reverse-transcribed with primers containing 12-nt unique molecular identifiers (UMIs). The UMIs tag each original molecule and allow correction of PCR amplification bias. Libraries were amplified for 19 PCR cycles, during which dual indices were added for multiplexing. Library size distribution and quality were assessed by capillary electrophoresis (TapeStation D1000; Agilent Technologies, Santa Clara, CA, USA). Libraries were quantified by qPCR, pooled in equimolar amounts, and sequenced on a NextSeq 500/550 system (Illumina, San Diego, CA, USA) with 75-bp single-end reads. Sequencing yielded an average of 35 million reads per sample, with a median Phred quality score > 30.

Sequencing data processing and differential expression analysis

miRNA sequencing analysis. Reads were processed with the QIAGEN GeneGlobe Data Analysis Center (QIAGEN, Aarhus, Denmark). Read processing and annotation: 1) Adapters (identified by the common sequence AACTGTAGGCACCATCAAT) and low-quality bases were trimmed, and UMIs were extracted from the demultiplexed reads. Reads shorter than 15 nt or longer than 55 nt were discarded; 2) Reads with identical UMIs, or UMIs differing by one nucleotide, were collapsed into a consensus sequence representing a single original molecule; 3) Consensus reads were annotated by sequential alignment to miRBase (v22.1), allowing up to 2 mismatches and isomiRs with start/end positions shifted by up to 2 nt, and then to piRNAdb (v1.7.6), tRNA sequences (release 19), and snoDB (v22). Differential expression was assessed with DESeq2 (v1.34.0) which models raw counts with a negative binomial distribution. The design included case–control pair and diagnosis. Three comparisons were made: all discovery subjects (17 MDD-S vs. 17 controls), males (10 vs. 10), and females (7 vs. 7). Because candidates

were to be validated in a second stage, miRNAs with a nominal $p < 0.05$ were considered differentially expressed (DEmiRs).

mRNA sequencing analysis. Protein-coding transcript fragments captured in small RNA libraries provide gene expression estimates comparable to total RNA-seq and to recover the expected inverse miRNA-target relationships when both are profiled from the same library[74,75]. We therefore used UMI-collapsed reads that did not map to small RNA databases to profile gene expression from the same libraries. Read quality was assessed with FastQC (v0.11.9) and summarized with MultiQC (v0.11.9). Reads were aligned to the human reference genome (GRCh38) using STAR (v2.7.6), and gene-level counts were obtained with featureCounts (v2.0.1). Count matrices were processed with edgeR (v3.36.0) in R (v4.1.2) and converted to counts per million (CPM) after TMM normalization, yielding 12,173 genes (10,529 protein-coding genes). Differential expression between MDD-S and control subjects was assessed separately in males (10 vs. 10) and females (7 vs. 7) using two-sided two-sample t-tests on CPM values. Student's t-test was used, or Welch's t-test when an F-test indicated unequal variances ($p < 0.05$). Protein-coding genes (Ensembl biotype "protein_coding") with a nominal $p < 0.05$ were considered differentially expressed genes (DEGs). As in the miRNA discovery phase, an uncorrected threshold was used to capture the modest changes expected from miRNA-mediated regulation and to prioritize sensitivity for validation. Log_2 fold changes (FC) were calculated as log_2(mean CPM in MDD-S / mean CPM in controls), and DEGs were classified as upregulated or downregulated according to their sign.

Sex-by-diagnosis interaction analysis. To test whether the effect of MDD-S differed between the sexes, we analyzed the 10,529 protein-coding genes quantified in the discovery cohort (10 male and 7 female case-control pairs). Gene biotypes were assigned from Ensembl release 110. CPM values were log_2-transformed after adding a pseudocount of 1. We used limma (v3.66.0) in R (v4.5.0) to fit a linear model with MDD-S - control pair as a fixed effect, diagnosis, and a diagnosis-by-sex interaction term (males as reference), using lmFit and eBayes with trend = TRUE and robust = TRUE. Because each pair comprised subjects of the same sex, the main effect of sex was absorbed by the pair term. The interaction coefficient represents the difference in the effect of MDD-S between females and males. This analysis was exploratory: a two-sided nominal $p < 0.05$ was considered significant. Separately, all protein-coding genes were classified as

significant only in males, only in females, or in both sexes with the same or opposite direction of change according to the per-sex differential expression test described above. For genes significant in only one sex, we defined four cumulative levels of evidence for sex specificity: Level 1: significant in one sex only; Level 2: additionally, a nominal interaction $p < 0.05$; Level 3: additionally, $p \geq 0.2$ in the per-sex t-test of the other sex; Level 4: additionally, $p \geq 0.5$ in the other sex, and an absolute $\log_2$FC ($\log_2$ ratio of mean CPM) in the other sex smaller than 25% of that in the sex showing the effect. The number of genes expected by chance in each category and level was estimated by permuting sex labels across the 17 pairs (2,000 permutations, preserving the 10/7 split) and repeating the full classification, including the interaction model. One-sided empirical p values were calculated as (1 + number of permutations with a count ≥ the observed count)/2,001. Internal reproducibility was assessed in 200 random splits of the pairs of each sex into discovery and held-out halves (discovery/held-out: 5/5 pairs in males and 4/3 in females). Genes were classified into categories and levels in the discovery half, applying the same tests to the discovery pairs only. For each gene, the between-sex difference in effect was defined as the $\log_2$FC ($\log_2$ ratio of mean CPM, calculated in the held-out pairs) in the sex showing the effect minus the $\log_2$FC in the other sex, multiplied by the sign of the discovery-half $\log_2$FC in the sex showing the effect. We calculated the proportion of genes in which this difference remained greater than zero in the held-out pairs and compared it with that obtained after permuting sex labels (500 permutations × 5 splits; one-sided empirical p = [1 + number of permutations with a mean proportion ≥ the observed one]/501).

Rank-rank hypergeometric overlap RRHO2 analysis of miRNA profiles. To compare MDD-associated changes in miRNA expression between the sexes without applying significance thresholds, we performed rank-rank hypergeometric overlap analysis with the RRHO2 package (v1.0) in R (v4.5.0). Differential expression statistics (MDD-S vs. control) for each sex were taken from the miRNA sequencing analysis described above, which accounted for the paired design. The analysis was restricted to the 1,702 miRNAs detected in both sexes, irrespective of their significance. Within each sex, miRNAs without a valid statistic were excluded. The remaining miRNAs were ranked by signed significance, $-\log_{10}(P) \times \text{sign}(\log_2 FC)$, using unadjusted p-values (p-values of 0 were replaced by the smallest positive double-precision number), so that rank 1 corresponded to the most upregulated miRNA in MDD-S. Overlap between the two ranked lists was

assessed with hypergeometric tests at successive rank thresholds in steps of 5 miRNAs (step size = 5; boundary = 0.01). P-values were adjusted across all pairs of thresholds using the Benjamini-Hochberg procedure implemented in RRHO2 (multipleTesting = "BH"). The resulting map shows $-\log_{10}$(adjusted P) (maximum observed value, 41.16; color scale capped at 40). Its four quadrants represent concordant (up-up, down-down) and discordant (up-down, down-up) overlap. The association between the ranking metrics of both sexes across all common miRNAs was quantified with Spearman's rank correlation (two-sided; $\rho = -0.386$, $p = 1.46 \times 10^{-61}$, n = 1,702).

Rank-rank hypergeometric overlap RRHO2 analysis of mRNA profiles. The same procedure, with the same ranking direction, multiple-testing correction, and quadrant definition, was applied to mRNAs, with the following differences. The analysis was restricted to the 10,529 protein-coding genes quantified in both sexes. To account for the paired design, gene-level statistics were computed specifically for this analysis: within each sex (10 male and 7 female MDD-S–control pairs), MDD-S and control samples were compared using two-sided paired *t*-tests on log2(CPM) values. Genes with fewer than three complete pairs or with zero variance in the paired differences were excluded. Genes were ranked by $-\log_{10}$(P) × sign (mean paired difference, MDD-S - control). RRHO2 was run with steps of 50 genes (stepsize = 50; boundary = 0.015). The maximum value on the map was 73.57 (color scale capped at 75), and Spearman's correlation was $\rho = -0.206$ ($p = 9.24 \times 10^{-102}$, n = 10,529).

Comparison with an independent dataset. NCBI-generated raw counts (GRCh38.p13) and sample metadata for the dlPFC (BA8/9) samples of Labonté et al.[22] were obtained from GEO (GSE102556). Within each sex, MDD-S cases were compared with controls (13 vs. 13 males; 13 vs. 9 females) using DESeq2 (1.50.2). The 15,700 protein-coding genes (Ensembl release 110) tested in both sexes were ranked by $-\log_{10}$(p-value) × sign($\log_2$FC) and analyzed with RRHO2 as described above (stepsize = 50; boundary = 0.015; Benjamini-Hochberg correction), and the association between sexes was quantified with Spearman's correlation ($\rho = -0.102$, $p = 1.77 \times 10^{-37}$).

Data visualization. Heatmaps show row-scaled z-scores of $\log_2$(TMM-normalized CPM + 1) for miRNAs and of $\log_2$(CPM + 1) for mRNAs; rows and columns were ordered by hierarchical clustering with 1 - Pearson correlation distance and Ward's linkage

(ward.D2). Heatmaps and Venn diagrams were generated in R (v4.5.0) with the ComplexHeatmap, VennDiagram and ggpubr packages, and volcano plots in GraphPad Prism (v10.0; GraphPad Software, San Diego, CA, USA).

RT-qPCR validation

Validation of candidate miRNAs. miRNA validation was performed in two steps. First, 37 candidate miRNAs, prioritized on the basis of read abundance, fold change (> 20%), documented expression in the brain and reported disease associations (HMDD v4.0)[34], were measured in the discovery cohort by QIAGEN Genomic Services. Total RNA (10 ng) was reverse-transcribed in 10 µl reactions using the miRCURY LNA RT Kit (QIAGEN). Synthetic RNA and DNA spike-ins (UniSp6 and UniSp3) were added to monitor reverse-transcription efficiency and PCR inhibition. The cDNA was diluted 100-fold and assayed in 10 µl reactions on a custom miRCURY LNA miRNA PCR Panel with miRCURY LNA SYBR Green Master Mix, on a LightCycler 480 RT-PCR System (Roche, Basel, Switzerland) in 384-well plates. Threshold cycles (Ct) were determined with the second-derivative maximum method (Roche LC software), and amplification specificity was verified by melting-curve analysis. Expression was normalized to the geometric mean of three reference miRNAs (miR-9-3p, miR-103a-3p, and miR-30e-5p).

Second, miRNAs that differed between groups in this first step were then measured in the extended cohort, separately in each sex, using an independent reverse-transcription chemistry. In both sexes, miRNAs with $p < 0.1$ in the paired comparison were selected. miR-1299 met this criterion in males but was not measured because no suitable primers could be designed for the poly(A)-based assay. In total, 15 miRNAs were measured in males and 13 in females. Total RNA (3 µg) was polyadenylated in 50 µl reactions containing 1.5 U of E. coli Poly(A) Polymerase (Thermo Fisher Scientific) and 1 mM ATP at 37 °C for 60 min, and the reaction was stopped on ice. Polyadenylated RNA was reverse-transcribed with 50 U of MultiScribe Reverse Transcriptase (Thermo Fisher Scientific) and an anchored oligo-dT adapter (5′-GCACGCTACGACCTCAGAGTCACTATGGCACTTTTTTTTTTTTTTTVN-3′; V = G, A, or C; N = G, A, T, or C) at 37 °C for 120 min, followed by inactivation at 85 °C for 5 min. Quantitative PCR was performed on an Applied Biosystems 7500 Real-Time PCR System (Thermo Fisher Scientific). Each 10 µl reaction contained PowerTrack SYBR Green Master Mix, cDNA equivalent to 2.5 ng of input RNA, 300 nM of a miRNA-specific forward primer, and a universal reverse primer complementary to the adapter

(**Table S9**). Cycling conditions were 95 °C for 2 min, followed by 40 cycles of 95 °C for 15 s and 60 °C for 60 s. Specificity was verified by melting-curve analysis (60–95 °C, 0.5 °C increments). All reactions were run in technical triplicate. Relative expression was calculated as $2^{-\Delta Ct}$, with ΔCt relative to the geometric mean Ct of four reference RNAs (miR-9-3p, miR-103a-3p, miR-30e-5p, and RNU6), whose stability in the dlPFC was confirmed with NormFinder and expressed relative to the mean of the control group.

Validation of target mRNAs. Selected target mRNAs were measured in the extended cohort. Total RNA (1 µg) was reverse-transcribed with the High-Capacity cDNA Reverse Transcription Kit (Thermo Fisher Scientific) using random hexamers (25 °C for 10 min, 37 °C for 120 min, and 85 °C for 5 min). RT-qPCR was performed on an Applied Biosystems 7500 system in technical triplicate. Each 10 µl reaction contained PowerTrack SYBR Green Master Mix, cDNA equivalent to 2.5 ng of input RNA, and 300 nM of each primer (**Table S10**). Cycling conditions and melting-curve analysis were as described for miRNAs. Relative expression was calculated as $2^{-\Delta Ct}$, with ΔCt relative to the geometric mean of *ACTB*, *GAPDH,* and *RPL13A*, and expressed relative to the mean of the control group.

Identification of experimentally validated miRNA targets and functional enrichment

To avoid the high false-positive rates of prediction algorithms, target identification was restricted to experimentally validated miRNA–mRNA interactions. Targets of the RT-qPCR-validated DEmiRs identified in each sex were retrieved from miRTarBase (v11.0; evidence types included, e.g., reporter assay, CLASH, microarray, CLIP-seq, western blot, qPCR, RNA-seq). Functional annotation of these target lists was performed with WebGestalt 2024 (WEB-based GEne SeT AnaLysis Toolkit) platform[76]. Over-representation analysis (ORA) was performed against the human protein-coding genome as the reference background to identify enriched KEGG pathways and Gene Ontology (GO) Biological Process (BP) and Molecular Function (MF) terms. Significance was assessed with hypergeometric tests and Benjamini–Hochberg correction ($p.adj < 0.05$). Pathways and terms unrelated to brain function (e.g., cancer- or infection-related pathways) were excluded, and among the remaining ones we prioritized those with the lowest adjusted *P* values, the highest enrichment ratios and the most direct relevance to brain function. Overlap among KEGG pathways was visualized in Cytoscape (v3.10.2)

as networks in which nodes represent pathways (size proportional to the number of target genes) and edges connect pathways with an overlap coefficient ≥ 0.20 (shared target genes / target genes of the smaller pathway). Edge thickness is proportional to the overlap coefficient. Pathways without edges above this threshold are not shown.

Construction of miRNA–mRNA regulatory networks

Sex-specific regulatory networks were built by integrating the miRNA and mRNA data. Only DemiRs confirmed by RT-qPCR in the extended cohort were included, and their direction of change was taken from these RT-qPCR measurements. For two miRNAs, this direction differed from that in the sequencing data (miR-4516 in males and miR-483-5p in females; **Tables S3 and S4**). Experimentally supported targets of these DEmiRs were retrieved from miRTarBase[37] and cross-referenced with the DEGs of the same sex. Because miRNAs typically repress their targets, only pairs with opposite directions of change were retained: upregulated miRNAs with downregulated target DEGs, and vice versa. Networks were visualized and analyzed in Cytoscape (v3.10.2) to identify regulatory hubs. Nodes color indicates $\log_2$ fold change (MDD vs. control), calculated from RT-qPCR in the extended cohort for miRNAs and from sequencing for mRNAs. To select candidate target genes for RT-qPCR, we examined the binding sites of each miRNA-target interaction reported in miRTarBase or, where not available there, in the original publications cited in miRTarBase, giving priority to interactions with complementarity in the miRNA seed region (nucleotides 2-8) in the 3′UTR or coding sequence of the target transcript.

Protein-protein interaction (PPI) network construction and module analysis

PPI networks were built from DEGs that were experimentally supported targets of the DEmiRs and changed in the opposite direction to them. Physical interaction networks were generated with Metascape (v3.5.20260701)[39], which integrates STRING, BioGRID, OmniPath, and InWeb_IM. Only physical interactions (physical score > 0.132) were included, and text-mining predictions were excluded. Networks were visualized in Cytoscape (v3.10.2) using the Prefuse Force Directed Layout (spring coefficient, 1×10^{-6}; default spring length, 400; default node mass, 15). Minor manual adjustments were made to improve legibility without altering network topology. Node size was scaled to degree, and node color indicates $\log_2$ fold change from sequencing.

Cell-type mapping of target genes

Target genes were mapped onto an independent single-nucleus RNA-seq (snRNA-seq) dataset of the human dlPFC (GEO: GSE213982)[23], which we reanalyzed in R (v4.1.2) with Seurat (v4.3.0.1). Data processing, clustering and cell-type annotation followed the procedures of the original study. We used the 41 cell-type clusters annotated in the original study and within-sex differential expression statistics ($\log_2$ fold change and Bonferroni-adjusted P values) for MDD cases versus controls, obtained with Wilcoxon rank-sum tests (Seurat FindMarkers). The analysis was restricted to DEGs that were experimentally supported targets of the DEmiRs and changed in the opposite direction to them. For each sex, a gene with $p.adj < 0.05$ in a cluster was considered differentially expressed in that cluster. Genes differentially expressed in a single cluster were classified as unique, and those differentially expressed in more than one cluster as shared. The direction of change of each gene was assigned from the sign of its mean $\log_2$ fold change across all clusters in which it was differentially expressed. Clusters were grouped into excitatory neurons, inhibitory neurons, glial and endothelial cells, and a mixed-lineage cluster, following the annotation of the original study.

Statistical analysis

Statistical models for sequencing data, sex-by-diagnosis interaction, threshold-free cross-sex comparisons (RRHO2 and Spearman's correlation), enrichment, and snRNA-seq analyses are described in the corresponding sections above. RT-qPCR data, correlations, and covariate analyses were analyzed with GraphPad Prism (v10.0). Data are presented as mean ± SEM. In box-and-whisker plots, the centre line indicates the median, box limits the 25th and 75th percentiles, and whiskers the minimum and maximum values. Normality was assessed with the Shapiro-Wilk test in each group, and outliers were identified and excluded with the ROUT method (Q = 1%); the corresponding pair was then excluded from paired tests. Comparisons between MDD and matched control subjects were performed with paired Student's t-tests or Wilcoxon matched-pairs signed-rank tests, depending on the data distribution. Unpaired comparisons were performed with unpaired *t*-test or Mann–Whitney U tests. Correlations were assessed with Spearman's rank correlation coefficients. These included correlations between sequencing and RT-qPCR data, between miRNA and target mRNA levels measured by RT-qPCR, and between transcript levels and covariates (age, PMI, and RIN). To test whether miRNA and target-gene changes in females differed by cause of death, we

compared MDD–control pairs in which the MDD subject died of natural causes (n = 6) with those in which the MDD subject died by suicide (n = 9). Within-pair ΔΔCt values (ΔCt of the MDD subject − ΔCt of the matched control) were analysed using Bayesian two-sample t-tests implemented in the BayesFactor R package (v0.9.12-4.8), with a default Cauchy prior (r = 0.707) and an equivalence interval for the standardized effect size of $-0.5 < \delta < 0.5$. Robustness was assessed across prior widths of r = 0.3–2. Evidence for equivalence was expressed as BF_{01} and interpreted as anecdotal (1–3), moderate (3–10), or strong (> 10)[77]. For single-gene comparisons, two-tailed $p < 0.05$ was considered significant, and $0.05 \leq P < 0.10$ was described as marginal.

References

1. Herrman, H. *et al.* Reducing the global burden of depression: a Lancet-World Psychiatric Association Commission. *Lancet Lond. Engl.* **393**, e42–e43 (2019).
2. Marwaha, S. *et al.* Novel and emerging treatments for major depression. *Lancet Lond. Engl.* **401**, 141–153 (2023).
3. Dwivedi, Y., Roy, B. & Korla, P. K. Genome-wide methylome-based molecular pathologies associated with depression and suicide. *Neuropsychopharmacology* **50**, 705–716 (2025).
4. Malhi, G. S. & Mann, J. J. Depression. *Lancet Lond. Engl.* **392**, 2299–2312 (2018).
5. Kern, D. M. *et al.* Suicide-specific mortality among patients with treatment-resistant major depressive disorder, major depressive disorder with prior suicidal ideation or suicide attempts, or major depressive disorder alone. *Brain Behav.* **13**, e3171 (2023).
6. Gonçalves Peter, A. *et al.* Incidence and Risk Factors for Suicide Attempts in Patients Diagnosed with Major Depressive Disorder. *Psychol. Res. Behav. Manag.* **13**, 1147–1157 (2020).
7. Hawton, K., Casañas I Comabella, C., Haw, C. & Saunders, K. Risk factors for suicide in individuals with depression: a systematic review. *J. Affect. Disord.* **147**, 17–28 (2013).
8. Pemau, A. *et al.* Symptomatic networks in suicide attempt and reattempt: Relevance of psychiatric comorbidity. *Eur. Psychiatry J. Assoc. Eur. Psychiatr.* **68**, e4 (2025).
9. Dobbertin, M. *et al.* Neuroimaging alterations of the suicidal brain and its relevance to practice: an updated review of MRI studies. *Front. Psychiatry* **14**, 1083244 (2023).
10. Malhi, G. S. *et al.* Cognitive and emotional impairments underpinning suicidal activity in patients with mood disorders: an fMRI study. *Acta Psychiatr. Scand.* **139**, 454–463 (2019).
11. Peng, W., Chen, Z., Yin, L., Jia, Z. & Gong, Q. Essential brain structural alterations in major depressive disorder: A voxel-wise meta-analysis on first episode, medication-naive patients. *J. Affect. Disord.* **199**, 114–123 (2016).
12. Thompson, C. & Ong, E. L. C. The Association Between Suicidal Behavior, Attentional Control, and Frontal Asymmetry. *Front. Psychiatry* **9**, 79 (2018).
13. Chen, M. *et al.* Heightened effective connectivity of DLPFC-mPFC and DLPFC-ACC circuits in major depressive disorder with suicidal ideation: evidence from a TMS-EEG study. *Transl. Psychiatry* **15**, 332 (2025).
14. Fries, G. R., Saldana, V. A., Finnstein, J. & Rein, T. Molecular pathways of major depressive disorder converge on the synapse. *Mol. Psychiatry* **28**, 284–297 (2023).
15. Duman, R. S., Aghajanian, G. K., Sanacora, G. & Krystal, J. H. Synaptic plasticity and depression: new insights from stress and rapid-acting antidepressants. *Nat. Med.* **22**, 238–249 (2016).
16. Kang, H. J. *et al.* Decreased expression of synapse-related genes and loss of synapses in major depressive disorder. *Nat. Med.* **18**, 1413–1417 (2012).
17. Li, J. *et al.* Cortical structural differences in major depressive disorder correlate with cell type-specific transcriptional signatures. *Nat. Commun.* **12**, 1647 (2021).
18. Yoshino, Y., Roy, B., Kumar, N., Shahid Mukhtar, M. & Dwivedi, Y. Molecular pathology associated with altered synaptic transcriptome in the dorsolateral prefrontal cortex of depressed subjects. *Transl. Psychiatry* **11**, 73 (2021).
19. Bagot, R. C. *et al.* Circuit-wide Transcriptional Profiling Reveals Brain Region-Specific Gene Networks Regulating Depression Susceptibility. *Neuron* **90**, 969–983 (2016).
20. Seney, M. L. *et al.* Opposite Molecular Signatures of Depression in Men and Women. *Biol. Psychiatry* **84**, 18–27 (2018).

21. Roy, B. & Dwivedi, Y. M6A RNA epitranscriptome dynamics linked to major depressive disorder and suicide risk. *Neuropsychopharmacol. Off. Publ. Am. Coll. Neuropsychopharmacol.* **50**, 1524–1535 (2025).
22. Labonté, B. *et al.* Sex-specific transcriptional signatures in human depression. *Nat. Med.* **23**, 1102–1111 (2017).
23. Maitra, M. *et al.* Cell type specific transcriptomic differences in depression show similar patterns between males and females but implicate distinct cell types and genes. *Nat. Commun.* **14**, 2912 (2023).
24. Mansouri, S. *et al.* Transcriptional dissection of symptomatic profiles across the brain of men and women with depression. *Nat. Commun.* **14**, 6835 (2023).
25. Nagy, C. *et al.* Single-nucleus transcriptomics of the prefrontal cortex in major depressive disorder implicates oligodendrocyte precursor cells and excitatory neurons. *Nat. Neurosci.* **23**, 771–781 (2020).
26. Rainville, J. R., Lipuma, T. & Hodes, G. E. Translating the Transcriptome: Sex Differences in the Mechanisms of Depression and Stress, Revisited. *Biol. Psychiatry* **91**, 25–35 (2022).
27. Bortolozzi, A., Manashirov, S., Chen, A. & Artigas, F. Oligonucleotides as therapeutic tools for brain disorders: Focus on major depressive disorder and Parkinson's disease. *Pharmacol. Ther.* **227**, 107873 (2021).
28. Lopez, J. P. *et al.* miR-1202 is a primate-specific and brain-enriched microRNA involved in major depression and antidepressant treatment. *Nat. Med.* **20**, 764–768 (2014).
29. Żurawek, D. & Turecki, G. The miRNome of Depression. *Int. J. Mol. Sci.* **22**, 11312 (2021).
30. Smalheiser, N. R. *et al.* MicroRNA expression is down-regulated and reorganized in prefrontal cortex of depressed suicide subjects. *PloS One* **7**, e33201 (2012).
31. Francis, A. & Dwivedi, Y. Integrative methylation and miRNA dysregulation in dlPFC reveal distinct molecular signatures of suicide and non-suicide subtypes in major depressive disorder. *Psychiatry Clin. Neurosci.* **80**, 757–764 (2026).
32. Yoshino, Y., Roy, B. & Dwivedi, Y. Differential and unique patterns of synaptic miRNA expression in dorsolateral prefrontal cortex of depressed subjects. *Neuropsychopharmacol. Off. Publ. Am. Coll. Neuropsychopharmacol.* **46**, 900–910 (2021).
33. Plaisier, S. B., Taschereau, R., Wong, J. A. & Graeber, T. G. Rank-rank hypergeometric overlap: identification of statistically significant overlap between gene-expression signatures. *Nucleic Acids Res.* **38**, e169 (2010).
34. Cui, C., Zhong, B., Fan, R. & Cui, Q. HMDD v4.0: a database for experimentally supported human microRNA-disease associations. *Nucleic Acids Res.* **52**, D1327–D1332 (2024).
35. Miquel-Rio, L. *et al.* Peripheral miRNA profiling identifies therapy-specific biological trajectories in the treatment of cognitive dysfunction in depression: an exploratory mechanistic study. *Sci. Rep.* https://doi.org/10.1038/s41598-026-55039-1 (2026) doi:10.1038/s41598-026-55039-1.
36. Liao, Y., Smyth, G. K. & Shi, W. featureCounts: an efficient general purpose program for assigning sequence reads to genomic features. *Bioinforma. Oxf. Engl.* **30**, 923–930 (2014).
37. Cui, S. *et al.* miRTarBase 2025: updates to the collection of experimentally validated microRNA–target interactions. *Nucleic Acids Res.* **53**, D147–D156 (2025).
38. Bartel, D. P. MicroRNAs: genomics, biogenesis, mechanism, and function. *Cell* **116**, 281–297 (2004).

39. Zhou, Y. *et al.* Metascape provides a biologist-oriented resource for the analysis of systems-level datasets. *Nat. Commun.* **10**, 1523 (2019).
40. Szklarczyk, D. *et al.* The STRING database in 2023: protein–protein association networks and functional enrichment analyses for any sequenced genome of interest. *Nucleic Acids Res.* **51**, D638–D646 (2022).
41. Espinosa Garcia, E. *et al.* Construction of miRNA-mRNA networks for the identification of lung cancer biomarkers in liquid biopsies. *Clin. Transl. Oncol. Off. Publ. Fed. Span. Oncol. Soc. Natl. Cancer Inst. Mex.* **25**, 643–652 (2023).
42. Goftari, S. N., Bahrami, A. R. & Matin, M. M. Integrated Analysis of lncRNA-miRNA-mRNA ceRNA Network and Identification of Hub lncRNAs in Molecular Subtypes of Gastric Cancer as Potential Prognostic Indicators. *Bioinforma. Biol. Insights* **20**, 11779322261433659 (2026).
43. Li, D. *et al.* Identification of circRNA/lncRNA-miRNA-Transcription Factor-mRNA Networks to Identify Potential Biomarkers in Response to Neoadjuvant Therapy for Breast Cancer. *Breast Cancer* **18**, 538948 (2026).
44. Yin, X. *et al.* Identification of Potential miRNA-mRNA Regulatory Network Contributing to Parkinson's Disease. *Park. Dis.* **2022**, 2877728 (2022).
45. Ray, A. *et al.* miRNA-mRNA Interaction Network Analysis in Alzheimer's Disease for Biomarker Discovery. *J. Mol. Neurosci. MN* **76**, 123 (2026).
46. Pantazatos, S. P. *et al.* Whole-transcriptome brain expression and exon-usage profiling in major depression and suicide: evidence for altered glial, endothelial and ATPase activity. *Mol. Psychiatry* **22**, 760–773 (2017).
47. Beckelman, B. C. *et al.* Dysregulation of Elongation Factor 1A Expression is Correlated with Synaptic Plasticity Impairments in Alzheimer's Disease. *J. Alzheimers Dis. JAD* **54**, 669–678 (2016).
48. Balamotis, M. A. *et al.* Satb1 ablation alters temporal expression of immediate early genes and reduces dendritic spine density during postnatal brain development. *Mol. Cell. Biol.* **32**, 333–347 (2012).
49. Wagnon, J. L. *et al.* CELF4 regulates translation and local abundance of a vast set of mRNAs, including genes associated with regulation of synaptic function. *PLoS Genet.* **8**, e1003067 (2012).
50. Lynes, E. M. *et al.* Palmitoylation is the switch that assigns calnexin to quality control or ER Ca2+ signaling. *J. Cell Sci.* **126**, 3893–3903 (2013).
51. Goes, F. S. *et al.* Large-scale transcriptomic analyses of major depressive disorder reveal convergent dysregulation of synaptic pathways in excitatory neurons. *Nat. Commun.* **16**, 3981 (2025).
52. Pucharcos, C., Estivill, X. & de la Luna, S. Intersectin 2, a new multimodular protein involved in clathrin-mediated endocytosis. *FEBS Lett.* **478**, 43–51 (2000).
53. Ba, W. *et al.* ARHGAP12 Functions as a Developmental Brake on Excitatory Synapse Function. *Cell Rep.* **14**, 1355–1368 (2016).
54. Lee, B. H., Meyer, C. M., Speca, D. J. & Díaz, E. Adhesion G-Protein Coupled Receptors in Neurological and Psychiatric Disorders. *J. Psychiatry Brain Sci.* **10**, e250017 (2025).
55. Vitobello, A. *et al.* ADGRL1 haploinsufficiency causes a variable spectrum of neurodevelopmental disorders in humans and alters synaptic activity and behavior in a mouse model. *Am. J. Hum. Genet.* **109**, 1436–1457 (2022).
56. Dumais, A. *et al.* Risk factors for suicide completion in major depression: a case-control study of impulsive and aggressive behaviors in men. *Am. J. Psychiatry* **162**, 2116–2124 (2005).

57. Richard-Devantoy, S., Berlim, M. T. & Jollant, F. A meta-analysis of neuropsychological markers of vulnerability to suicidal behavior in mood disorders. *Psychol. Med.* **44**, 1663–1673 (2014).
58. Huang, J. *et al.* Repression of p53 activity by Smyd2-mediated methylation. *Nature* **444**, 629–632 (2006).
59. Xu, G. *et al.* The Histone Methyltransferase Smyd2 Is a Negative Regulator of Macrophage Activation by Suppressing Interleukin 6 (IL-6) and Tumor Necrosis Factor α (TNF-α) Production. *J. Biol. Chem.* **290**, 5414–5423 (2015).
60. Elabi, O. F. *et al.* Deletion of RGS5 attenuates high-fat diet-induced cerebrovascular pathology and associated spatial memory deficits. *Brain. Behav. Immun.* **138**, 106950 (2026).
61. Yin, S. *et al.* RGS5 augments astrocyte activation and facilitates neuroinflammation via TNF signaling. *J. Neuroinflammation* **20**, 203 (2023).
62. Genç, Ö. *et al.* MCTP is an ER-resident calcium sensor that stabilizes synaptic transmission and homeostatic plasticity. *eLife* **6**, e22904.
63. Marano, G. *et al.* Neuroinflammation and the Female Brain: Sex-Specific Mechanisms Underlying Mood Disorders and Stress Vulnerability. *Life* **16**, 139 (2026).
64. Kropp, D. R. & Hodes, G. E. Sex differences in depression: An immunological perspective. *Brain Res. Bull.* **196**, 34–45 (2023).
65. Dion-Albert, L. *et al.* Vascular and blood-brain barrier-related changes underlie stress responses and resilience in female mice and depression in human tissue. *Nat. Commun.* **13**, 164 (2022).
66. Lee, Y.-F. *et al.* Premature aging with impaired oxidative stress defense in mice lacking TR4. *Am. J. Physiol. Endocrinol. Metab.* **301**, E91-98 (2011).
67. Kang, H. S. *et al.* Nuclear orphan receptor TAK1/TR4-deficient mice are protected against obesity-linked inflammation, hepatic steatosis, and insulin resistance. *Diabetes* **60**, 177–188 (2011).
68. Carneiro, B. A. *et al.* MicroRNAs as Diagnostic Biomarkers and Predictors of Antidepressant Response in Major Depressive Disorder: A Systematic Review. *Cureus* **16**, e56910 (2024).
69. He, Y., Houtenbos, S. & Wippert, P.-M. Differentially expressed microRNAs in human depression: a systematic review of case-control and longitudinal studies. *BMC Psychiatry* **25**, 624 (2025).
70. Šalamon Arčan, I., Katrašnik, M., Kouter, K., Zupanc, T. & Videtič Paska, A. Extracellular vesicles from cerebrospinal fluid revealed changes in miR-19a-3p and miR-4516 expression in Slovene male suicides. *Genes Brain Behav.* **22**, e12868 (2023).
71. Bondjers, C. *et al.* Transcription profiling of platelet-derived growth factor-B-deficient mouse embryos identifies RGS5 as a novel marker for pericytes and vascular smooth muscle cells. *Am. J. Pathol.* **162**, 721–729 (2003).
72. Garcia, F. J. *et al.* Single-cell dissection of the human cerebrovasculature in health and disease. *Nature* **603**, 893–899 (2022).
73. De Prisco, M. & Vieta, E. The never-ending problem: Sample size matters. *Eur. Neuropsychopharmacol. J. Eur. Coll. Neuropsychopharmacol.* **79**, 17–18 (2024).
74. Azadova, A., Ekperuoh, A., Brooke, G. N. & Marco, A. Analysis of coding gene expression from small RNA sequencing. *Genome Res.* **36**, 611–618 (2026).
75. Akat, K. M. *et al.* Detection of circulating extracellular mRNAs by modified small-RNA-sequencing analysis. *JCI Insight* **5**, e127317, 127317 (2019).

76. Elizarraras, J. M. *et al.* WebGestalt 2024: faster gene set analysis and new support for metabolomics and multi-omics. *Nucleic Acids Res.* **52**, W415–W421 (2024).
77. van Ravenzwaaij, D., Monden, R., Tendeiro, J. N. & Ioannidis, J. P. A. Bayes factors for superiority, non-inferiority, and equivalence designs. *BMC Med. Res. Methodol.* **19**, 71 (2019).

Acknowledgements

Grateful acknowledgment is extended to the brain donors and to the staff members of the Basque Institute of Legal Medicine for their collaboration in the study. Furthermore, we would like to thank Laura Clavaín (Ego Genomics) for her assistance in the interpretation of the transcriptomic analyses and support with the single-cell data analysis.

Author contributions

A.B. conceived the original idea for the study; L.M.R. and A.B planned and oversaw all aspects of the study; L.M.R. and J.J.E. performed and analyzed most of the experiments; V.P. and E.R.B. performed the RNA isolation and first-strand cDNA synthesis experiments and provided technical support to most of the experiments; L.F.C. and J.J.M. managed the collection of human brain samples; M.V.G., M.J.P, J.D.A., and C.F. contributed to the statistical analyses and interpretation of the findings, as well as provided the necessary resources G.T. and E.V. critically reviewed the manuscript and contributed to the interpretation of the results. L.M.R and A.B. wrote the manuscript with input and substantial revisions from all authors. All authors reviewed and approved the final manuscript.

Funding

This work was supported by MCIU/AEI/FEDER, UE grant (PID2022-141700OB-I00, MCIN/AEI/https://doi.org/10.13039/501100011033 to A.B.), ISCIII (PI20/00270 to M.J.P.), Fundació La Marató de TV3 and Generalitat de Catalunya (202207-30-31-32 to A.B., and 202227-30 to M.J.P.), and AGAUR 2021-SGR-01358 to A.B. and 2021-SGR-00832 to M.J.P. of the Generalitat de Catalunya. We also thank the Basque Government (IT1512/22 and IT1920/26) and Spanish Stress Research Network, MCIN/AEI /https://doi.org/10.13039/501100011033, and Centre for Biomedical Research in Mental Health Network (CIBERSAM). J.J.E. is a recipient of a pre-doctoral fellowship (FPU24/01721) from the Spanish Government. L.M.R. acknowledges financial support from the Spanish Ministry of Science, Innovation and Universities through the Juan de la Cierva 2024 postdoctoral fellowship (Grant JDC2024-053903-I).

Data

The small RNA sequencing data generated in this study (raw FASTQ files and processed miRNA and gene count matrices) have been submitted to the Gene Expression Omnibus (GEO) will be provided as soon as it is assigned and before publication. The previously published datasets analyzed in this study are available in GEO under accession codes GSE213982 (snRNA-seq of the human dlPFC; Maitra et al.[23]) and GSE102556 (bulk RNA-seq of the human dlPFC; Labonté et al.[22]). Source data are provided with this paper. Any additional information is available from the corresponding author upon reasonable request.

Code availability

Custom R scripts used for the RRHO2, sex-by-diagnosis interaction, permutation and Bayesian equivalence analyses, and for the reanalysis of the Labonté et al.[22] dataset, are available in Zenodo (https://doi.org/10.5281/zenodo.23769723). All other analyses were performed with publicly available software, as described in the Methods.

Declarations

Ethics approval and consent to participate

Human brain samples were collected at autopsy in the Basque Institute of Legal Medicine (Bilbao, Spain), in accordance with the applicable Spanish legal framework for postmortem human tissue studies, including Royal Decree 1716/2011. Samples were stored in an authorized brain repository registered at the Instituto de Salud Carlos III (Register C35). The study was approved by the Ethics Committee of the Spanish National Research Council (CSIC; approval no. 118/2021 Ref. PID2019-105136RB-I00). All procedures were conducted in accordance with the relevant ethical and legal requirements for research using postmortem human biological samples, and only anonymized, non-identifiable data were used for the analyses.

Consent for publication

Not applicable. This study was performed using anonymized postmortem human brain tissue and does not include identifiable individual data, images, or videos.

Competing interests

J.D.A. has served as consultant, advisor or CME speaker for Johnson & Johnson, Lundbeck, Pfizer, Neuraxpharm, Exeltis, Esteve and Viatris, outside the submitted work. EV has received grants and served as consultant, advisor or CME speaker for the following entities: AB-Biotics, Abbott, AbbVie, Adamed, Adium, Alcediag, Angelini, Biogen, Beckley-Psytech, Biohaven, Boehringer-Ingelheim, Bristol-Myers-Squibb, Casen-Recordati, Celon Pharma, Compass, Dainippon Sumitomo Pharma, Eli-Lilly, Engrail, Esteve, Ethypharm, Ferrer, Gedeon Richter, GH Research, Glaxo-Smith Kline, HMNC, Intra-Cellular therapies, Idorsia, Johnson & Johnson, LB pharmaceuthicals, Lundbeck, Luye Pharma, Medincell, Merck, Mitsubishi Tanabe Pharma, Newraxpharm, Newron, Novartis, Organon, Orion Corporation, Otsuka, Roche, Rovi, Sage, Sanofi-Aventis, Signant Health, Sunovion, Takeda, Teva, and Viatris, outside the submitted work. The other authors declare that they have no known competing financial interests or personal relationships that could have appeared to influence the work reported in this paper.

Table 1. Demographic and clinical characteristics of the study cohorts

Discovery cohort (n = 34)	**Control (n = 17)**		**MDD-S (n = 17)**	
Sex	**Male**	**Female**	**Male**	**Female**
Number of subjects	10	7	10	7
Age (years)	38.4 ± 3.8	40.9 ± 5.7	38.8 ± 3.7	40.3 ± 5.5
PMI (h)	15.0 ± 3.1	18.4 ± 1.6	18.4 ± 3.6	19.0 ± 1.9
RIN	7.3 ± 0.3	7.0 ± 0.2	6.8 ± 0.3	6.8 ± 0.4
Antidepressant detected (n)	0	0	3	3
Cause of death (n)	Accident (9), natural (1)	Accident (3), natural (4)	Suicide (10)	Suicide (7)
Additional samples (n = 36)	**Control (n = 18)**		**MDD (n = 18)**	
Sex	**Male**	**Female**	**Male**	**Female**
Number of subjects	10	8	10	8
Age (years)	44.7 ± 5.2	62.0 ± 4.5	44.7 ± 5.3	62.4 ± 4.3
PMI (h)	12.4 ± 2.2	19.2 ± 3.0	22.5 ± 3.0[a]	14.8 ± 3.2
RIN	7.5 ± 0.3	7.1 ± 0.2	7.5 ± 0.2	7.1 ± 0.3
Antidepressant detected (n)	0	0	3	3
Cause of death (n)	Accident (7), natural (3)	Accident (4), natural (4)	Suicide (10)	Suicide (2), natural (6)
Extended cohort (n = 70)	**Control (n = 35)**		**MDD (n = 35)**	
Sex	**Male**	**Female**	**Male**	**Female**
Number of subjects	20	15	20	15
Age (years)	41.5 ± 3.2	52.1 ± 4.5	41.8 ± 3.2	52.1 ± 4.5
PMI (h)	13.7 ± 1.9	18.9 ± 1.7	20.4 ± 2.3[b]	16.7 ± 1.9
RIN	7.4 ± 0.2	7.0 ± 0.2	7.1 ± 0.2	7.0 ± 0.3
Antidepressant detected (n)	0	0	6	6
Cause of death (n)	Accident (16), natural (4)	Accident (7), natural (8)	Suicide (20)	Suicide (9), natural (6)

The discovery cohort was used for small RNA sequencing and RT-qPCR technical validation. The extended cohort, comprising the discovery cohort and the additional samples, was used for RT-qPCR validation of miRNAs and target genes. Each MDD subject was matched to a control subject of the same sex. All subjects were of European ancestry. Values are mean ± SEM. or number of subjects. Antidepressant detected, number of subjects in whom antidepressants were detected by postmortem toxicological screening. MDD and control subjects were compared within each sex using paired Student's *t*-tests or Wilcoxon matched-pairs signed-rank tests, according to the normality of paired differences (Shapiro–Wilk). [a]$p = 0.019$ and [b]$p = 0.020$ vs. matched controls (paired *t*-test); all other comparisons, $p > 0.05$. MDD-S, MDD subjects who died by suicide; PMI, postmortem interval; RIN, RNA integrity number.

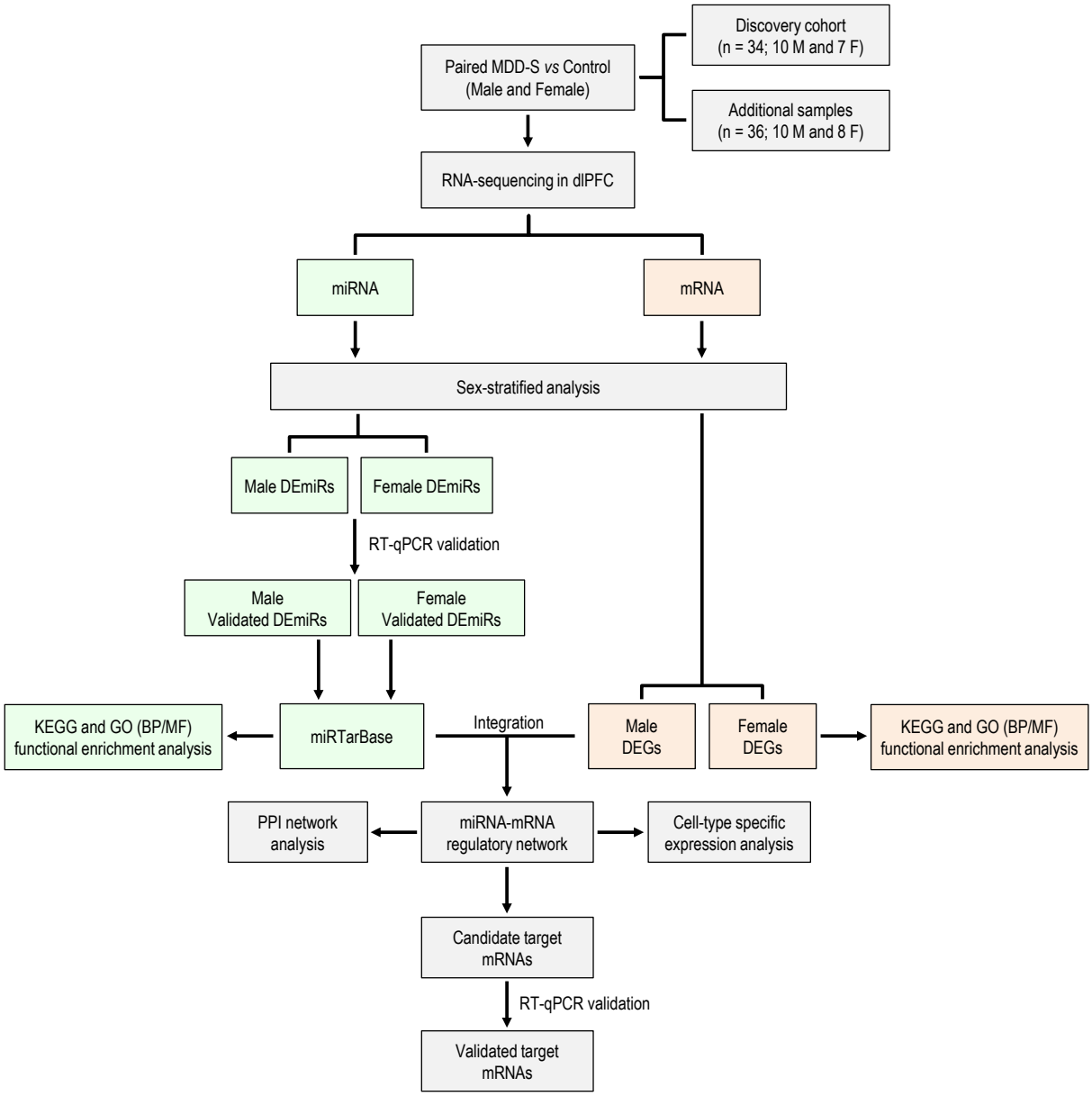


Figure 1. Study design and integrative multi-omic pipeline. Flowchart of the experimental and bioinformatic workflow used to identify sex-specific miRNA-mRNA regulatory networks in the dorsolateral prefrontal cortex (dlPFC) of individuals with major depressive disorder who died by suicide (MDD-S) and matched controls. Small RNA sequencing was performed in a discovery cohort of 17 MDD-S/control pairs (n = 34; 10 male [M] and 7 female [F] pairs); mRNA expression was profiled from reads of the same libraries that did not map to small RNA databases. Sex-stratified analyses identified differentially expressed miRNAs (DEmiRs) and genes (DEGs). DEmiRs were validated by RT-qPCR in the discovery plus an extended cohort of 18 pairs (n = 36; 10 M and 8 F pairs); total n = 70. Experimentally supported targets of validated DEmiRs were retrieved from miRTarBase and integrated with DEGs to build sex-stratified, directed miRNA-mRNA regulatory networks, which were further characterized by protein-protein interaction (PPI) analysis and cell-type-specific expression mapping using an independent single-nucleus RNA-seq (snRNA-seq) dataset. KEGG and Gene Ontology (biological process and molecular function) enrichment analyses were performed for miRNA targets and DEGs. Candidate target mRNAs selected from the networks were validated by RT-qPCR.

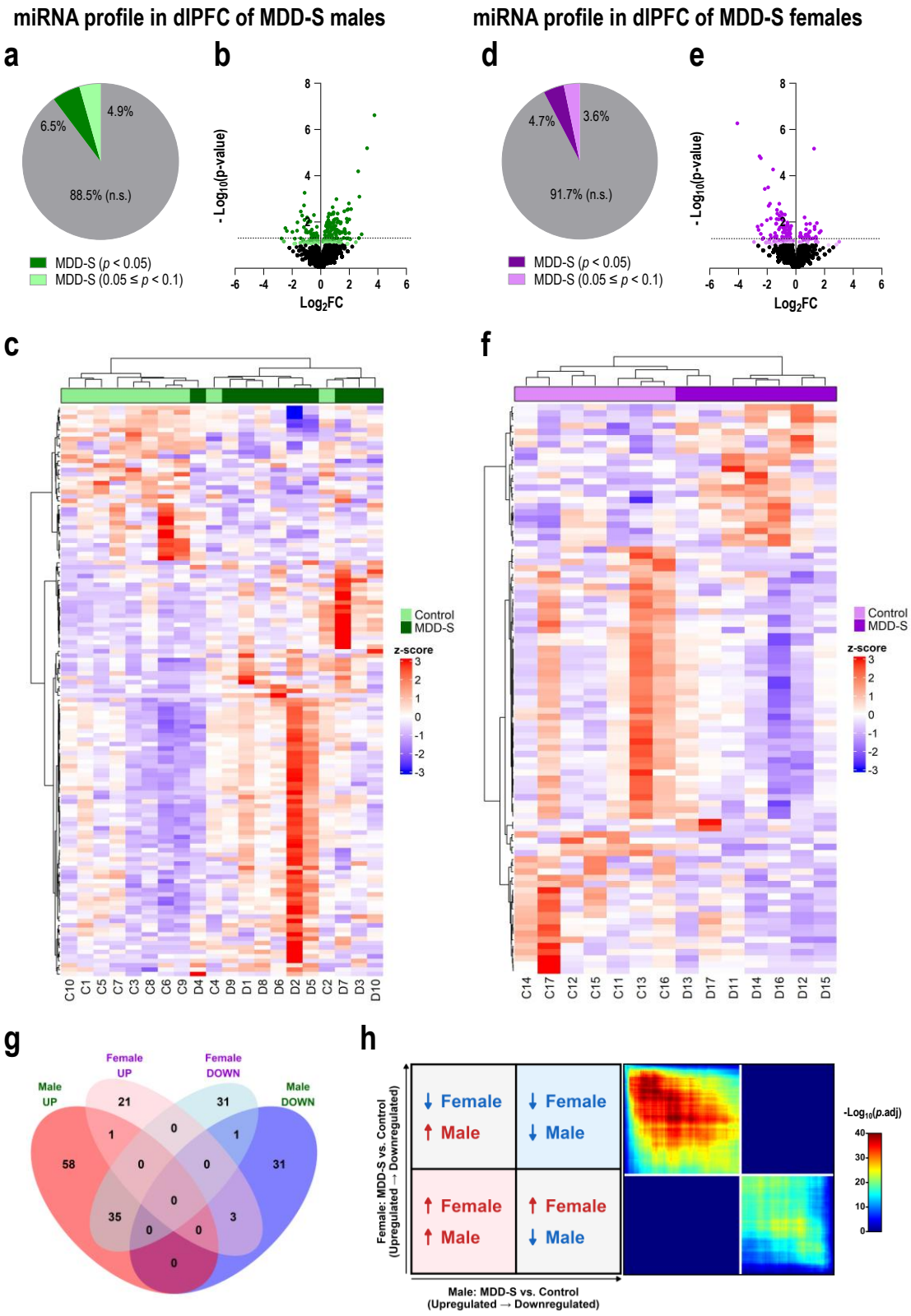


Figure 2. Sex-dependent and largely opposite miRNA expression changes in the dlPFC of individuals with MDD-S. **a, d** Pie charts showing the proportion of detected miRNAs that were differentially expressed (DEmiRs; $p < 0.05$) or marginally significant miRNAs ($0.05 \leq p < 0.1$) in MDD-S vs. control subjects in males (a; 10 vs. 10) and females (d; 7 vs. 7) of the discovery cohort. **b, e** Volcano plots showing $\log_2$ fold change

and -$\log_{10}$ p-value for each miRNA in males (b) and females (e); the dashed line indicates $p = 0.05$. **c, f** Heatmaps of DEmiRs in males (c) and females (f). Values are row-scaled z-scores of $\log_2$ (TMM-normalized CPM + 1); rows (miRNAs) and columns (subjects) were ordered by hierarchical clustering (1 - Pearson correlation distance, Ward's linkage; ComplexHeatmap, R). C, control; D, MDD-S; numbers correspond to pair ID in Supplementary Table 1. The color scale is capped at ± 3. **g** Venn diagram showing the overlap of up- and downregulated DEmiRs between males and females. **h** Rank–rank hypergeometric overlap (RRHO2) of transcriptome-wide miRNA differential expression in males (x-axis) and females (y-axis), ranked from upregulated to downregulated in MDD-S by -log10(p-value) × sign(log2 fold change); the color scale shows $-\log_{10}$ adjusted p-value of the overlap (capped at 40; maximum, 41.2). The schematic indicates the direction of change represented by each quadrant. . Spearman $\rho = -0.386$, $p = 1.46 \times 10^{-61}$. Differential expression was assessed with DESeq2, including case–control pair and diagnosis in the model; DEmiRs were defined as nominal $p < 0.05$. Source data are provided as a Source Data file.

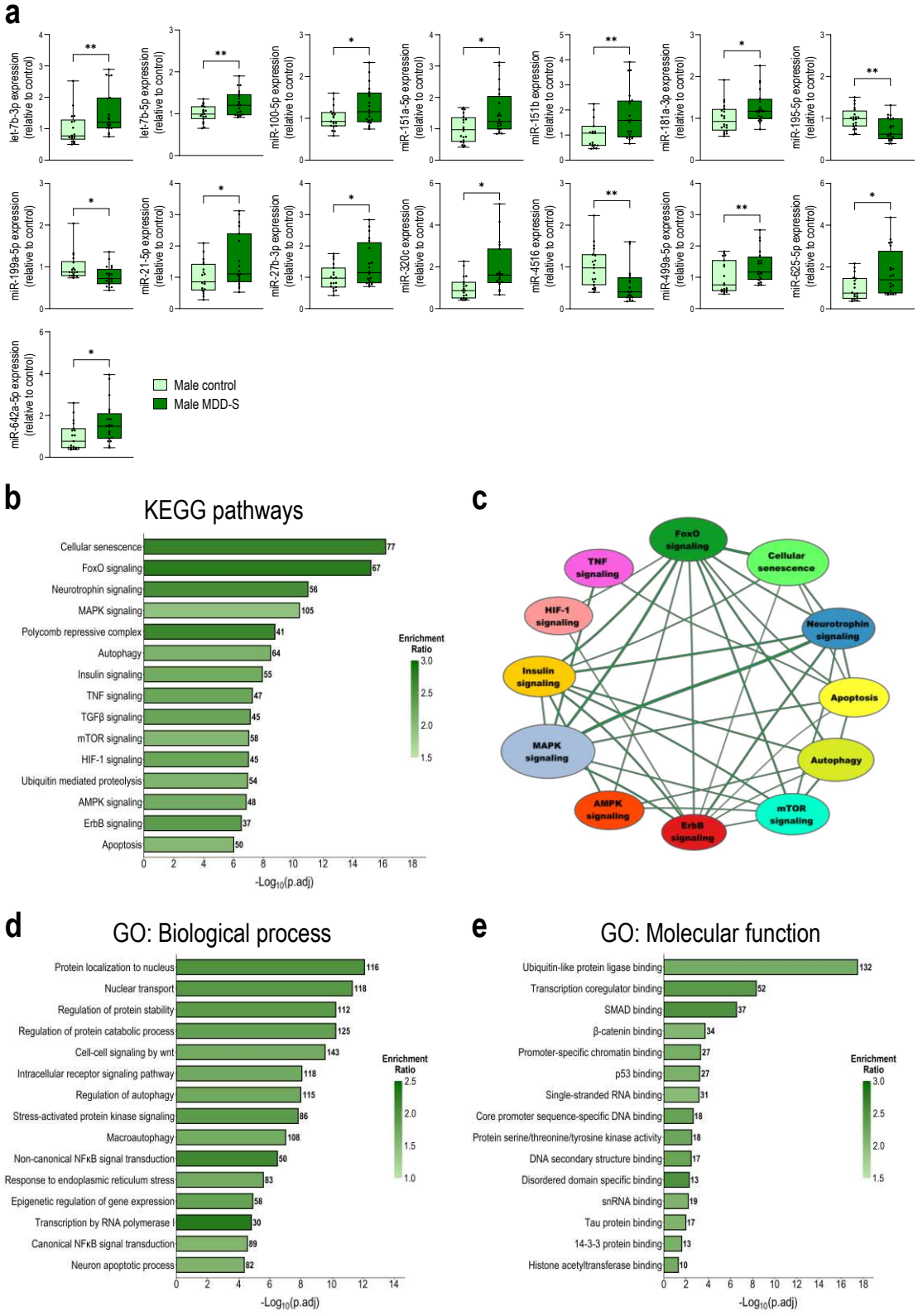


Figure 3. RT-qPCR validation and functional enrichment of male DEmiRs. **a** RT-qPCR validation of DEmiRs in the dlPFC of males from the discovery and extended cohorts (n = 20 MDD-S-control pairs). All 15 male DEmiRs were confirmed. Relative expression was calculated as $2^{-\Delta Ct}$, with ΔCt relative to the geometric mean of four reference RNAs (miR-9-3p, miR-103a-3p, miR-30e-5p, and RNU6), and normalized to

the mean of the control group. Box plots show the median and interquartile range; whiskers indicate minimum and maximum values; dots represent individual subjects. Outliers were identified with the ROUT method (Q = 1%) and removed. Values lacking a matched counterpart (e.g., because the paired sample was excluded) are shown but were not included in paired tests. Normality of paired differences was assessed in each group with the Shapiro–Wilk test, and groups were compared with a paired Student's *t*-test or Wilcoxon matched-pairs signed-rank test, as appropriate. *$p < 0.05$, **$p < 0.01$. **b** Selected KEGG pathways enriched among experimentally validated targets (miRTarBase) of the validated male DEmiRs (all with $p.adj < 0.05$). **c** Network of enriched KEGG pathways shown from b. Edges connect pathways with an overlap coefficient ≥ 0.20 (shared target genes / target genes of the smaller pathway), and edge width is proportional to the overlap. Pathways without connections above this threshold are not shown. **d, e** Gene Ontology (GO) biological process (d) and molecular function (e) terms enriched among the same targets, selected as in b. In **b**, **d** and **e**, bar length indicates -$\log_{10}$ adjusted p-value, bar color indicates enrichment ratio, and numbers show the number of target genes per term. Over-representation analysis used a hypergeometric test with Benjamini–Hochberg correction ($p.adj < 0.05$). Source data are provided as a Source Data file.

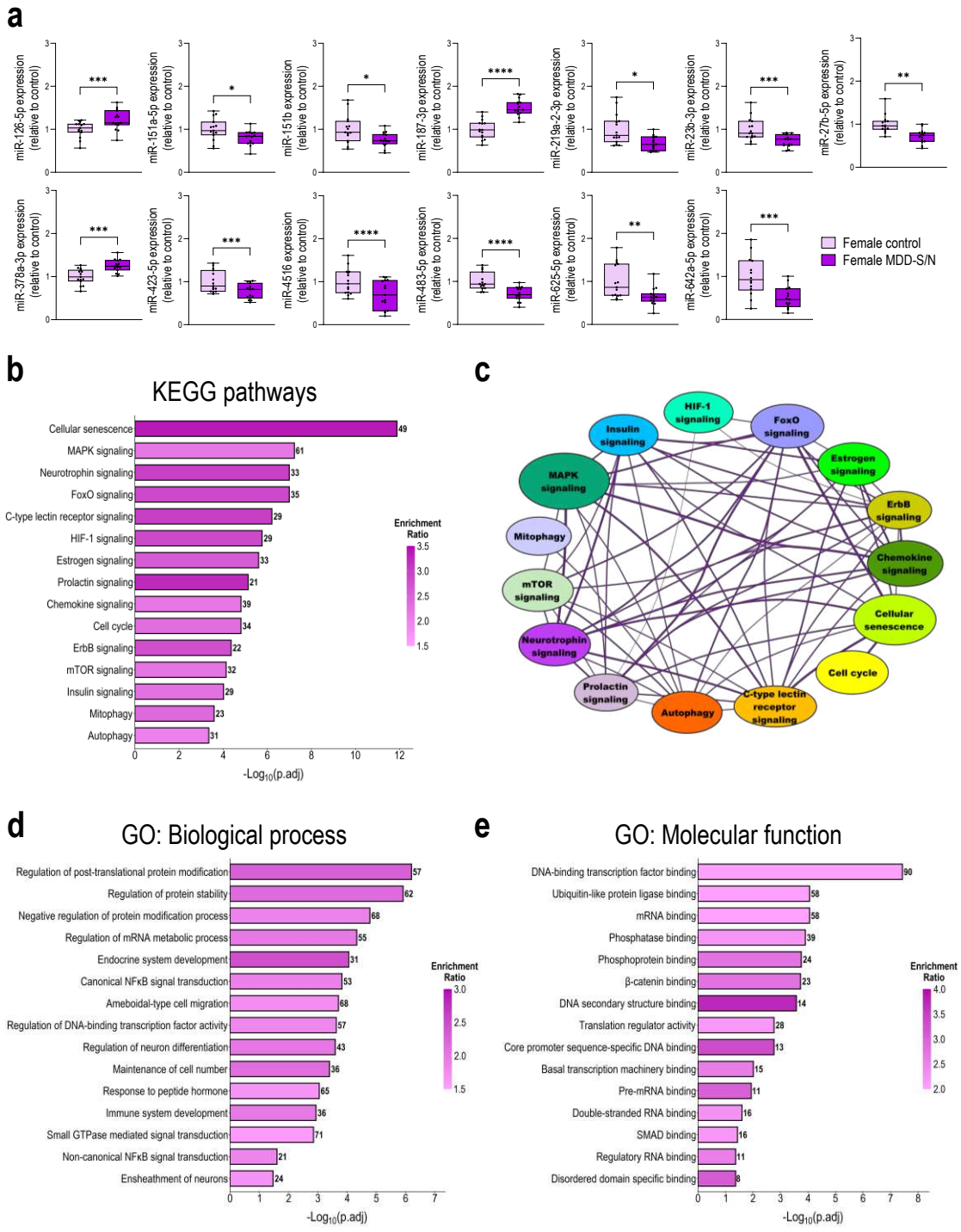


Figure 4. RT-qPCR validation and functional enrichment of female DEmiRs. **a** RT-qPCR validation of DEmiRs in the dlPFC of females from the discovery and extended cohorts (n =15 MDD-S/N-control control pairs). All 13 female DEmiRs were confirmed. Relative expression was calculated as $2^{-\Delta Ct}$, with ΔCt relative to the geometric mean of four reference RNAs (miR-9-3p, miR-103a-3p, miR-30e-5p, and RNU6), and expressed relative to the mean of the control group. Box plots show the median and interquartile range; whiskers indicate minimum and maximum values; dots represent individual subjects. Outliers were identified with the ROUT method (Q = 1%) and removed. Values

lacking a matched counterpart (e.g., because the paired sample was excluded) are shown but were not included in paired tests. Normality of paired differences was assessed in each group with the Shapiro–Wilk test, and groups were compared with a paired Student's *t*-test or Wilcoxon matched-pairs signed-rank test, as appropriate. **p* < 0.05, ***p* < 0.01, ****p* < 0.001, *****p* < 0.0001. **b** Selected KEGG pathways enriched among experimentally validated targets (miRTarBase) of the validated male DEmiRs (all with *p.adj* < 0.05). **c** Network of enriched KEGG pathways shown from b. Edges connect pathways with an overlap coefficient ≥ 0.20 (shared target genes / target genes of the smaller pathway), and edge width is proportional to the overlap. **d, e** Gene Ontology (GO) biological process (d) and molecular function (e) terms enriched among the same targets, selected as in b. In **b**, **d** and **e** bar length indicates $-\log_{10}$ adjusted p-value, bar color indicates enrichment ratio, and numbers show the number of target genes per term. Over-representation analysis used a hypergeometric test with Benjamini–Hochberg correction (*p.adj* < 0.05). Source data are provided as a Source Data file.

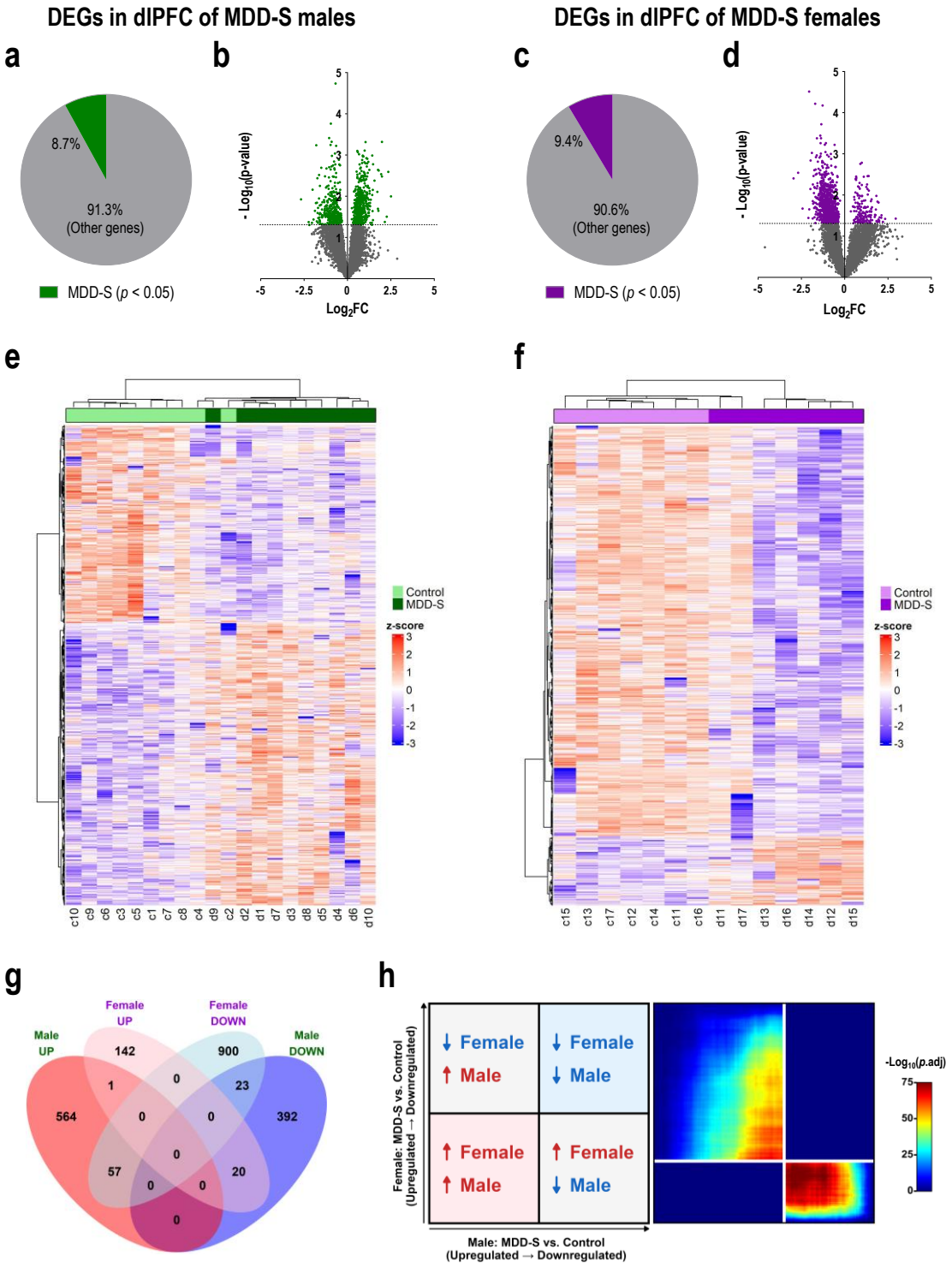


Figure 5. Sex-stratified gene expression profiles reveal opposite transcriptomic changes in the dlPFC of males and females with MDD-S. a, c Proportion of protein-coding DEGs ($p < 0.05$) among all 12,173 genes tested in males (a; 10 MDD-S, 10 controls) and females (c; 7 MDD-S, 7 controls); the remaining fraction comprises non-significant genes and non-coding genes with $p < 0.05$. **b, d** Volcano plots of $\log_2$ fold change (mean CPM in MDD-S / mean CPM in controls) versus -$\log_{10}$ p-value in males (b) and females (d). Protein-coding DEGs are colored and non-significant genes of all biotypes are shown in grey. The dashed line indicates nominal $p = 0.05$. **e, f** Heatmaps of

DEGs in males (e) and females (f). Values are row-scaled z-scores of $\log_2$ (CPM + 1); samples and genes were clustered by hierarchical clustering (1 - Pearson correlation distance, Ward's linkage). The color scale is capped at ± 3. C, control; D, MDD-S; numbers correspond to pair ID (Supplementary Table 1). **g** Overlap and direction of DEGs between sexes. **h** RRHO2 map comparing male and female gene rankings ($-\log_{10}$ p-value × sign of the mean paired difference, from two-sided paired t-tests on $\log_2$ CPM); 10529 protein-coding genes common to both sexes. Color indicates $-\log_{10}$ Benjamini-Hochberg-adjusted hypergeometric p (color scale at 75; maximum 73.5). Spearman $\rho = -0.206$, $p = 9.2 \times 10^{-102}$. In a–g, *p* values are nominal (uncorrected) and were obtained with two-sided Student's or Welch's t-tests on CPM values. Source data are provided as a Source Data file.

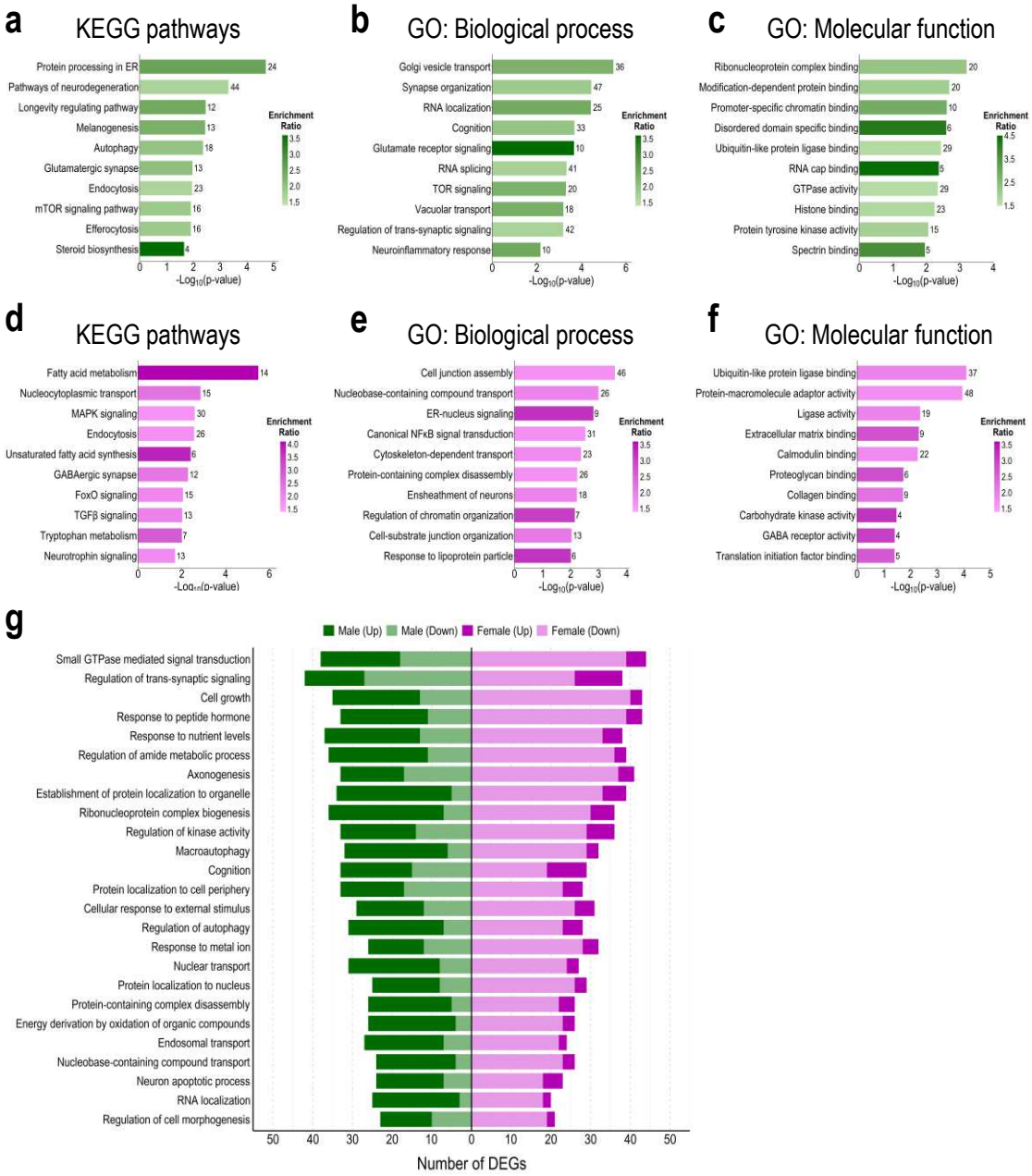


Figure 6. Functional characterization of male-only and female-only DEGs. a-c Selected KEGG pathways (a), GO biological processes (b), and GO molecular functions (c) enriched among the 956 DEGs found only in males. **d-f** KEEG pathways (d), GO biological processes (e), and GO molecular functions (f) enriched among the 1,042 DEGs found only in females. In each panel, 10 pathways or terms were selected from all those with nominal $p < 0.05$ and were ordered by p-value. In **a–f**, bar length indicates $-\log_{10}$ p-value, bar color indicates enrichment ratio, and numbers indicate the number of DEGs annotated to each term. Over-representation analysis (WebGestalt) used a hypergeometric test against the human protein-coding genome. Terms with FDR < 0.05 (Benjamini–Hochberg): protein processing in the ER (a); Golgi vesicle transport, synapse organization, RNA localization, cognition and glutamate receptor signaling (b); fatty acid metabolism (d); ubiquitin-like protein ligase binding and protein–macromolecule adaptor

activity (f); none in c and e. **g** Number of upregulated and downregulated male-only (left) and female-only (right) DEGs annotated to the 25 GO biological with the most DEGs among the 35 enriched in both sexes (Supplementary Table 8). Source data are provided as a Source Data file.

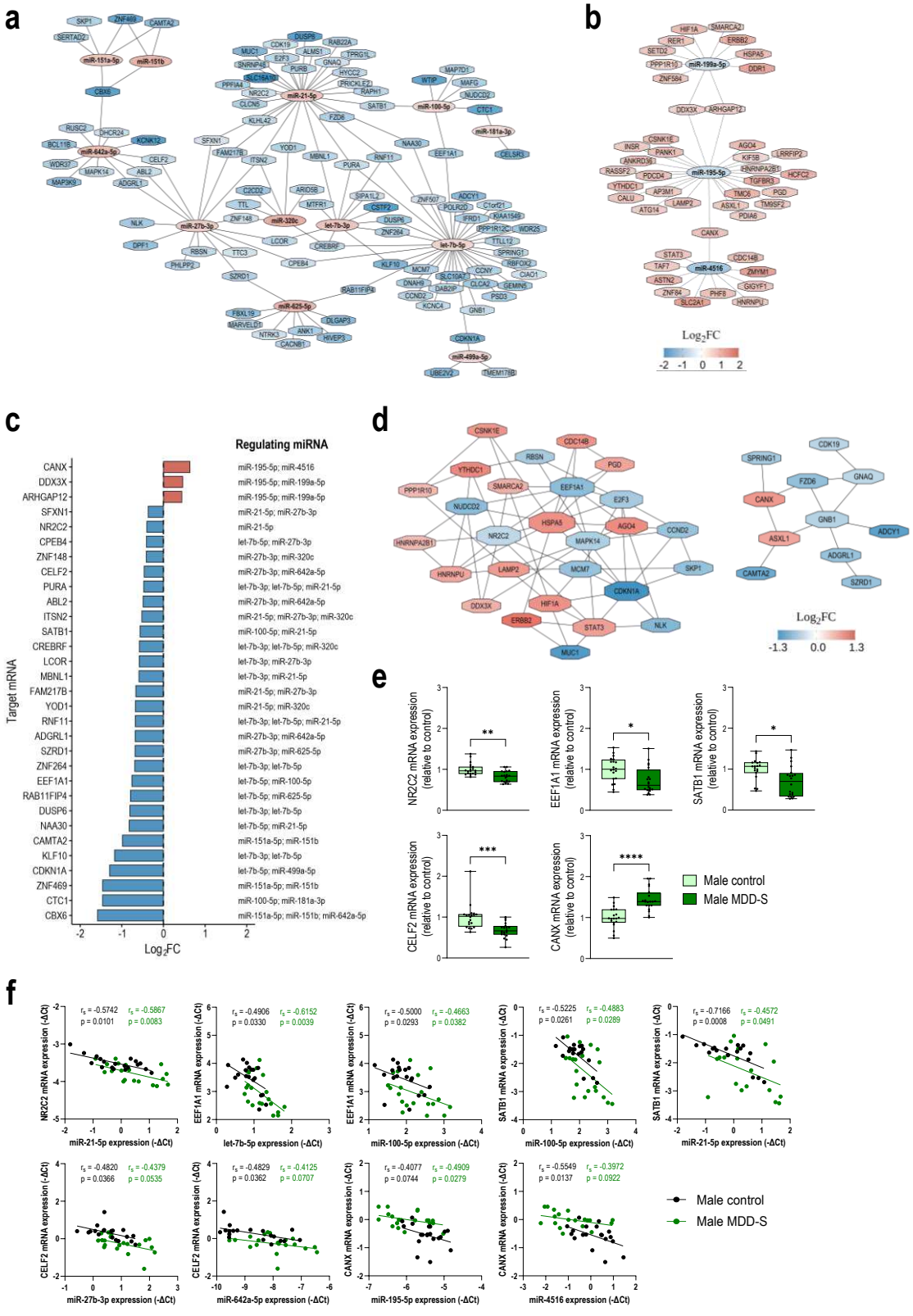


Figure 7. miRNA-mRNA regulatory networks in the male dlPFC and experimental validation of targets. a, b Regulatory networks linking RT-qPCR-validated male DEmiRs to their experimentally supported targets (miRTarBas, v11.0) among male DEGs that changed in the opposite direction: upregulated miRNAs and downregulated mRNAs (a), and downregulated miRNAs and upregulated mRNAs (b). Ellipses, miRNAs;

octagons, mRNAs; color indicates $\log_2$ fold change (MDD-S vs. control) by RT-qPCR for miRNAs and by sequencing data for mRNAs. **c** Log_2 fold change of selected target mRNAs and their regulating miRNAs. **d** Protein-protein interaction network of target genes from **a** and **b** (Metascape; physical interactions); color indicates $\log_2$ fold change and node size indicates degree. **e** RT-qPCR validation of selected targets in the dlPFC of 20 male MDD-S/control pairs from the extended cohort. Relative expression was calculated as $2^{-\Delta Ct}$, with ΔCt relative to the geometric mean of *ACTB*, *RPL13A* and *GAPDH,* and expressed relative to the mean of the control group. Box plots show the median and interquartile range; whiskers indicate minimum and maximum values; dots represent individual subjects. Outliers were identified with the ROUT method (Q = 1%) and removed. Values lacking a matched counterpart (e.g., because the paired sample was excluded) are shown but were not included in paired tests. Groups were compared with a paired Student's *t*-test or Wilcoxon matched-pairs signed-rank test according to the normality of each groups (Shapiro–Wilk). *$p < 0.05$, **$p < 0.01$, ***$p < 0.001$, ****$p < 0.0001$. **f** Correlation between RT-qPCR expression levels (-ΔCt) of validated miRNAs and their target mRNAs in control (black) and MDD-S (green) males. Spearman's rs and p-values are shown separately for each group; regression lines are shown for visualization only. Source data are provided as a Source Data file.

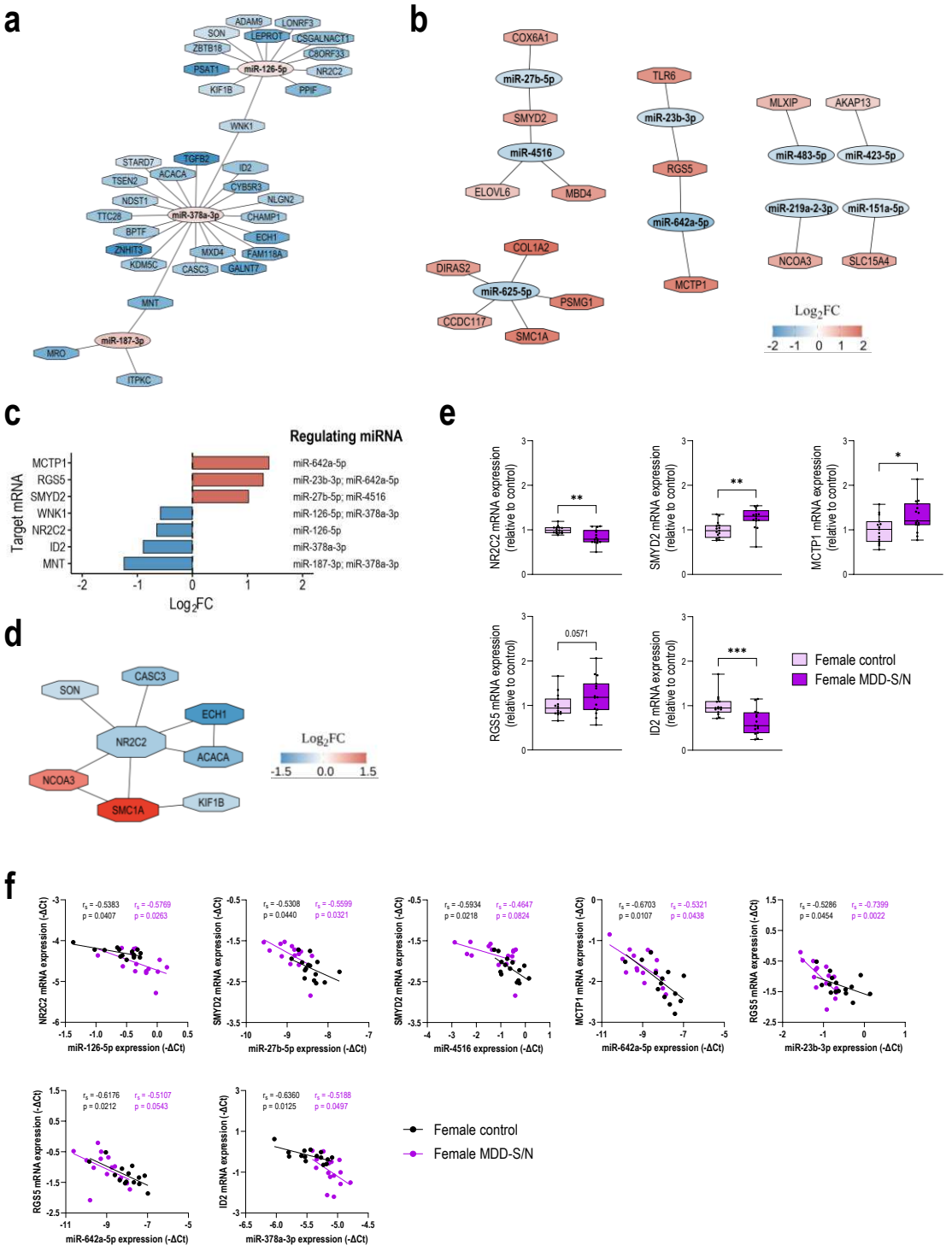


Figure 8. miRNA-mRNA regulatory networks in the female dlPFC and experimental validation. a, b Regulatory networks linking RT-qPCR-validated female DEmiRs to their experimentally supported targets (miRTarBase v11.0) among female DEGs that changed in the opposite direction: upregulated miRNAs and downregulated mRNAs (a), and downregulated miRNAs and upregulated mRNAs (b). miR-151b had no target among female DEGs and is not shown. Ellipses, miRNAs; octagons, mRNAs; color indicates $\log_2$ fold change (MDD-S/N vs. control) by RT-qPCR for miRNAs and by sequencing data for mRNAs. **c** Log_2 fold change of selected target mRNAs and their

regulating miRNAs. **d** Protein–protein interaction network of target genes from **a** and **b** (Metascape; physical interactions); color indicates $\log_2$ fold change and node size indicates degree. **e** RT-qPCR validation of selected targets in the dlPFC of 15 female MDD/control pairs (9 MDD-S and 6 MDD-N) from the extended cohort. Relative expression was calculated as $2^{-\Delta Ct}$, with ΔCt relative to the geometric mean of *ACTB*, *RPL13A* and *GAPDH,* and expressed relative to the mean of the control group. Box plots show the median and interquartile range; whiskers indicate minimum and maximum values; dots represent individual subjects. Outliers were identified with the ROUT method (Q = 1%) and removed. Values lacking a matched counterpart (e.g., because the paired sample was excluded) are shown but were not included in paired tests. Groups were compared with a paired Student's *t*-test or Wilcoxon matched-pairs signed-rank test according to the normality of each groups (Shapiro-Wilk). *$p < 0.05$, **$p < 0.01$. **f** Correlation between RT-qPCR expression levels (-ΔCt) of validated miRNAs and their target mRNAs in control (black) and MDD-S/N (purple) females. Spearman's rs and p-values are shown separately for each group; regression lines are shown for visualization only. MDD-S/N, MDD subjects who died by suicide or from natural causes. Source data are provided as a Source Data file.

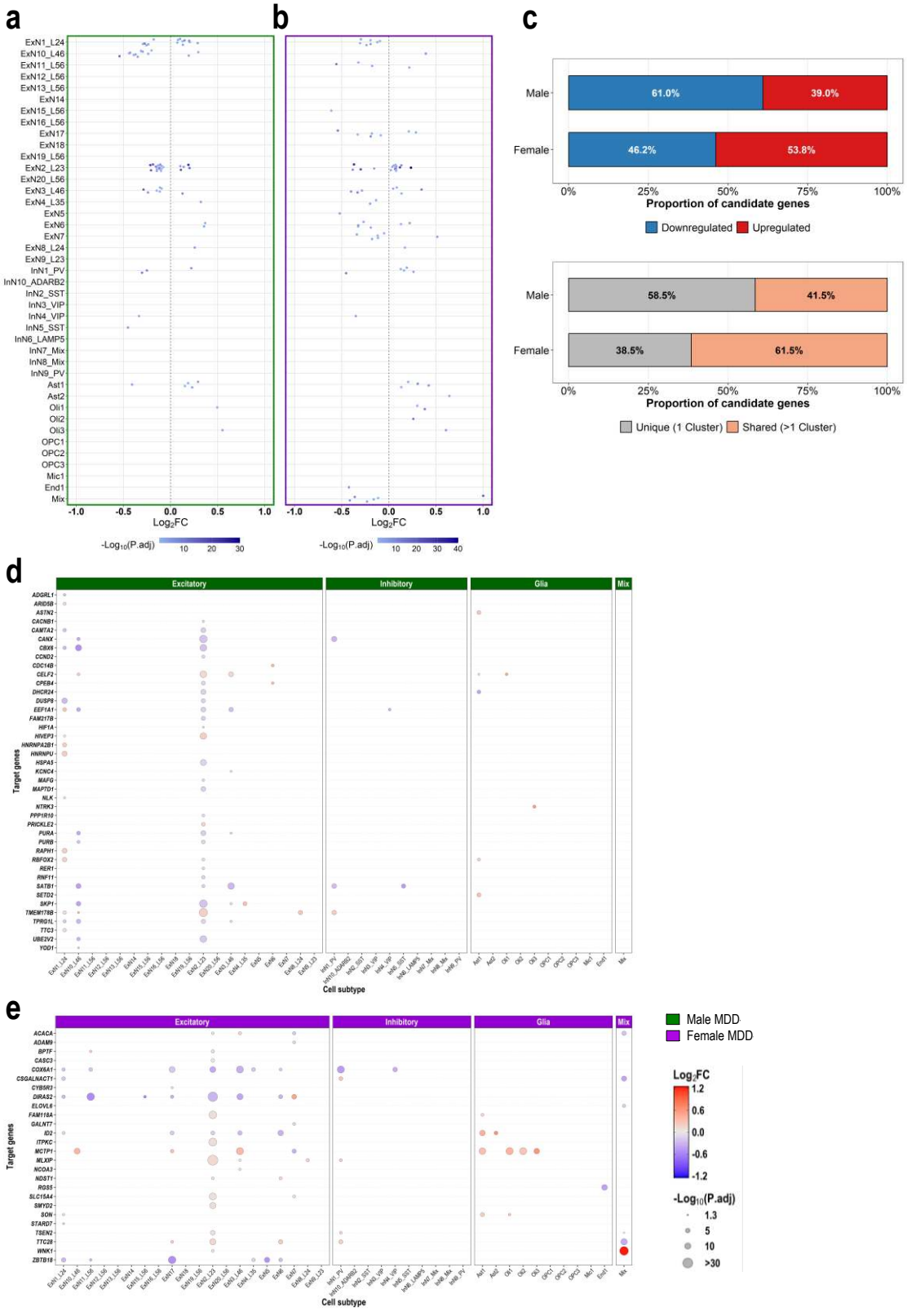


Figure 9. Mapping of network target genes onto dlPFC cell types in an independent snRNA-seq dataset. Target genes from the male and female miRNA–mRNA networks (Figs. 7a, b and 8a, b) were examined in a published snRNA-seq dataset of the human dlPFC (GEO: GSE213982; 160,711 nuclei from 71 donors)[23]. The dataset was re-analysed using the 41 cell-type clusters annotated in the original study; within each sex

and cluster, MDD and control nuclei were compared with Wilcoxon rank-sum tests (Seurat FindMarkers), and genes with Bonferroni-adjusted $p < 0.05$ are shown. **a, b** Log_2 fold change of target genes differentially expressed in each cluster in males (a; 41 of 147 targets) and females (b; 26 of 49 targets). Each dot represents one gene in one cluster; color indicates $-\log_{10}$ *p.adj*. **c** Proportion of these genes that were downregulated or upregulated (top), and that were differentially expressed in a single cluster or in more than one cluster (bottom); direction was assigned from the mean $\log_2$ fold change across the clusters in which each gene was differentially expressed. **d, e** Expression changes of the target genes across clusters in males (d) and females (e), grouped into excitatory neurons, inhibitory neurons, glial and endothelial cells, and a mixed cluster. Dot color indicates $\log_2$ fold change, and dot size indicates $-\log_{10}$ p-value (smallest dot, *p.adj* = 0.05). ExN, excitatory neurons; InN, inhibitory neurons; Ast, astrocytes; Oli, oligodendrocytes; OPC, oligodendrocyte precursor cells; Mic, microglia; End, endothelial cells; Mix, mixed-lineage cluster; L, cortical layers; PV, parvalbumin; SST, somatostatin; VIP, vasoactive intestinal peptide. Source data are provided as a Source Data file.

Supplementary Files

This is a list of supplementary files associated with this preprint. Click to download.

- SupplementaryTable2.docx
- SupplementaryTable6.docx
- Supplementarydata4.xlsx
- SupplementaryTable4.docx
- nrreportingsummary.pdf
- DescriptionofAdditionalSupplementaryFiles.pdf
- SuplementaryFigures.docx
- SupplementaryTable7.docx
- SupplementaryTable3.docx
- Supplementarydata3.xlsx
- SourceData.xlsx
- SupplementaryTable9.docx
- SupplementaryData5.xlsx
- SupplementaryTable8.docx
- SupplementaryData6.xlsx
- SupplementaryTable5.docx
- SupplementaryData1.xlsx
- SupplementaryTable1.docx
- SupplementaryData2.xlsx
- SupplementaryTable10.docx